GENETICS

Cosegregation of recombinant chromatids maintains genome-wide heterozygosity in an asexual nematode

Caroline Blanc[1]†, Nathanaelle Saclier[2]†, Ehouarn Le Faou[3], Lucas Marie-Orleach[3], Eva Wenger[1], Celian Diblasi[2], Sylvain Glemin[3,4], Nicolas Galtier[2], Marie Delattre[1]*

In asexual animals, female meiosis is modified to produce diploid oocytes. If meiosis still involves recombination, this is expected to lead to a rapid loss of heterozygosity, with adverse effects on fitness. Many asexuals, however, have a heterozygous genome, the underlying mechanisms being most often unknown. Cytological and population genomic analyses in the nematode *Mesorhabditis belari* revealed another case of recombining asexual being highly heterozygous genome-wide. We demonstrated that heterozygosity is maintained despite recombination because the recombinant chromatids of each chromosome pair cosegregate during the unique meiotic division. A theoretical model confirmed that this segregation bias is necessary to account for the observed pattern and likely to evolve under a wide range of conditions. Our study uncovers an unexpected type of non-Mendelian genetic inheritance involving cosegregation of recombinant chromatids.

INTRODUCTION

Asexual animal species are composed of females, which produce diploid daughters without paternal genome contribution. Asexuality requires the production of diploid oocytes and, hence, a modified female meiosis. Asexuality, which is derived from sexuality, has emerged multiple times and independently over the course of evolution, and many routes to producing diploid oocytes have been documented (*1*–*3*).

Depending on the type of cellular modification, different genetic outcomes are expected (Fig. 1A). A common prediction is that most modifications should lead to loss of heterozygosity (LOH). For some species, the entire meiotic program is achieved as in sexual species; however, the final haploid nucleus undergoes a duplication event (gamete duplication), which immediately generates a homozygous individual (Fig. 1A, b). When there is homologous recombination and one of the two meiotic divisions fails, either because the division is abortive or because the products of meiosis fuse back, LOH is also expected either distally or proximally to the crossover location (Fig. 1A, c and d). Hence, maintenance of heterozygosity is theoretically expected only in species for which meiotic recombination is largely reduced or totally abolished (*4*).

LOH is expected to negatively affect fitness because of the exposure of recessive deleterious mutations at diploid state. This has been suggested as a potential cause of the relative scarcity of asexual organisms in nature (*5*) and a selective pressure for reduced recombination rates in asexuals (*6*). Species that maintain some level of heterozygosity do not expose deleterious mutations and as such may circumvent some of the drawbacks of asexuality. In agreement with this expectation, a number of asexual lineages display appreciable amounts of heterozygosity (*7*–*10*). Yet, except in species for which a total loss of recombination has been demonstrated [for instance, (*11*, *12*)], the mechanisms of heterozygosity maintenance are still debated (*7*). Therefore, there is still a need to confront the cytological description and empirical genome data to reach a clear understanding of the genomic and cellular constraints in asexual animals.

We explored the mechanism of meiosis in the auto-pseudogamous nematode *Mesorhabditis belari* (Fig. 1B) (*13*). In this species, a female produces mainly diploid oocytes, which, although fertilized by a sperm, develop only from the maternal DNA and become females. This is also referred to as pseudogamy or sperm-dependent parthenogenesis. The same female also produces ~10% of haploid oocytes through regular meiosis, which, once fertilized, undergo fusion of the parental genomes. These amphimictic diploid embryos will give rise to males because active sperm cells always carry a Y chromosome (*13*). Hence, this species produces 90% asexual females and 10% sexual males. The males are needed to activate the oocytes that will mainly develop as asexual females, and for this reason, this reproductive strategy has been called auto-pseudogamy (*13*).

In this peculiar system, *M. belari* females have most likely maintained recombination for the production of regular oocytes (for the rare males). Given this constraint, we asked which modification of meiosis has been selected to produce the unreduced oocytes (for the asexual females) and with which genomic consequence for the species.

RESULTS

Diploid oocytes of *M. belari* are formed after failure of the first meiotic division

We first determined which steps of meiosis were modified to produce diploid oocytes in *M. belari*. We followed meiosis, making use of the spatiotemporal organization of the gonad, as found in the well-studied *Caenorhabditis elegans* species and other Rhabditidae nematodes (Fig. 2A). We had previously shown that this species is diploid and carries $2n = 20$ holocentric chromosomes (*13*). First, analysis of oocytes in diakinesis revealed that the

[1]Laboratory of Biology and Modeling of the Cell, Ecole Normale Supérieure de Lyon, CNRS UMR 5239, Inserm U1293, University Claude Bernard Lyon 1, Lyon, France. [2]Institut des Sciences de l'Evolution, Université Montpellier, Institut de Recherche pour le Développement, 34090 Montpellier, France. [3]University of Rennes, CNRS, ECOBIO (Ecologie, Biodiversité, Evolution)–UMR 6553, F-35000 Rennes, France. [4]Department of Ecology and Genetics, Evolutionary Biology Centre, Uppsala University, 75236 Uppsala, Sweden.
*Corresponding author. Email: marie.delattre@ens-lyon.fr
†These authors contributed equally to this work.

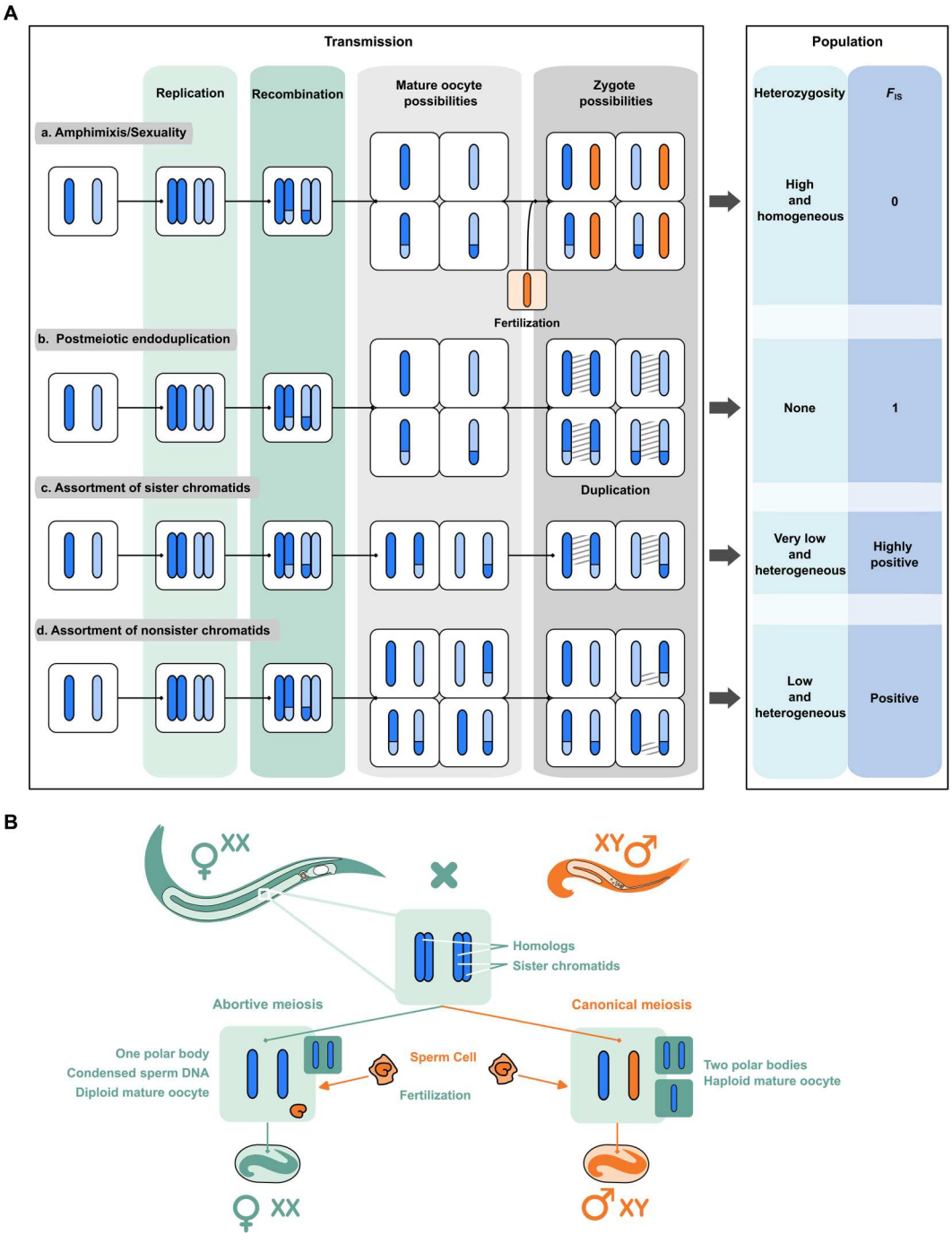

Fig. 1. Genetic expectation upon modification of meiosis in asexuals and reproductive system of *Mesorhabditis belari*. (**A**) Description of the expected genetic composition of a zygote and of a population upon different types of modifications of the meiotic program (b to d), often referred to as automixis. By contrast, in amphimictic reproduction, i.e., in regular sexual species, a canonical meiotic division generates a haploid set of maternal chromosomes (in blue), which fuse with the haploid paternal chromosomes (in orange) (a). Each bar represents a chromatid. Dark and light blue correspond to homologous chromosomes in oocytes. (b to d) Upon recombination, assortment of chromatids after modification of meiosis generates stretches of homozygosity, shown with hatching. Consequently, the level of heterozygosity in the population (right column) is decreased. The coefficient of inbreeding (F_{IS}) measures the excess of homozygosity compared to the Hardy-Weinberg expectation (i.e., in a randomly mating population); positive F_{IS} means an excess of homozygotes. Note that assortment of nonsister chromatids (d) is often referred to as "central fusion" (i.e., fusion of the two first products of meiosis), because it is genetically identical, although a fusion of meiotic products is not necessarily the cause of this type of unreduced meiosis. Similarly, assortment of sister chromatids (c) is generally referred to as "terminal fusion." (**B**) Schematic representation of the reproductive system found in *M. belari* as described in (*13*). Females (in green) produce two types of oocytes. Through canonical meiosis, a single chromatid per chromosome is transmitted to the oocyte (in blue). The sperm provides in single chromatid (in orange). The resulting diploid individuals give rise to males. Ninety percent of the oocytes are however diploid (incomplete meiosis, on the left) in which case the sperm does not contribute DNA because the sperm DNA is set aside after fertilization. These individuals give rise to females.

20 chromosomes were always paired into 10 units ($n > 200$ oocytes). Moreover, many bivalents had a crossed-shape structure (Fig. 2A), which resemble the chiasmata of holocentric chromosomes found in *C. elegans* (*14*, *15*), strongly suggesting that chromosomes undergo homologous recombination in *M. belari*.

Next, we reconstructed the different steps of meiotic divisions (Fig. 2, B and C). We found, as is the case for *C. elegans*, that oocytes are arrested at prometaphase of meiosis I, and meiosis resumes after fertilization. The long axis of the bivalents is oriented parallel to the spindle axis, as expected for holocentric chromosomes in regular meiosis (Fig. 2C) (*14*). In the Rhabditidae sexual species studied so far, a polar body is extruded at each meiotic division. The polar bodies are easily recognizable as tiny cells at the edge of the embryo (*16*). We had previously shown that all pseudogamous embryos in *M. belari* (i.e., developing from the unreduced oocytes) had only one polar body demonstrating that one meiotic

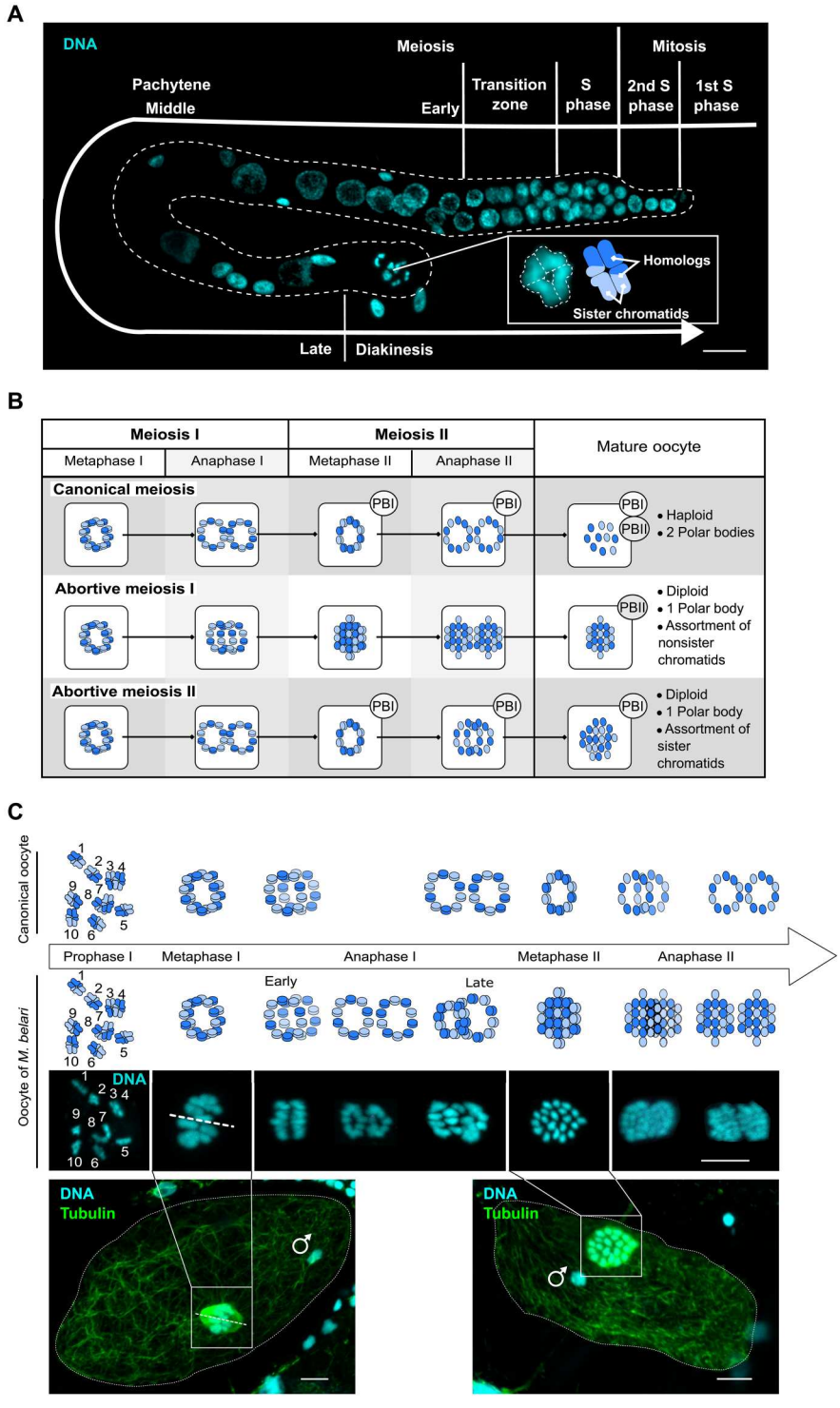

Fig. 2. Cytological evidence of abortive meiosis I in *M. belari* females. (**A**) Gonad of an *M. belari* female stained for DNA, showing the progression of meiotic cells along the tract. *M. belari* is diploid, carrying 2*n* = 20 chromosomes. Oocytes in diakinesis are found on the proximal part, with chiasmatic chromosomes. DNA is in blue. Scale bar, 20 µm. The holocentric bivalent chromosomes show a typical cross shape. The bivalents are schematized in blue, one chromosome is in dark blue, and its homolog is shown in light blue. (**B**) Expected patterns of chromosome organization upon failure of meiosis I or meiosis II in *M. belari*. A canonical meiosis is shown on the top. At metaphase, chromosomes orient as a ring. During anaphase, chromosomes (anaphase I) or chromatids (anaphase II) segregate as two rings. PB represents the polar body. (**C**) Reconstitution of *M. belari* meiosis in amphimictic (canonical meiosis) and pseudogamous (incomplete meiosis) embryos from fixed samples. On the bottom, representative pseudogamous embryos from which the images are taken. A sperm DNA is visible, although it will remain condensed and will not fuse with the female DNA. The polar body has not been extruded yet. Tubulin is in green, and DNA is in blue. The dotted line represents the long axis of the meiotic spindle along which the bivalent chromosomes align. Scale bars, 5 µm.

division was suppressed (*13*). We reasoned that if meiosis I was abortive, the 10 bivalents should dissociate into 20 univalents and no polar body should be detected at this stage. These univalents should next enter anaphase of meiosis II, showing two times 20 DNA-stained bodies (Fig. 2B). In contrast, if meiosis I was successful, a polar body would be extruded, and the 10 univalents would disassemble into 20 units corresponding to 20 sister chromatids after failure of meiosis II (Fig. 2B). We found many cells showing a metaphase plates containing 20 DNA-stained bodies. We also detected anaphase figures with two times 20 DNA-stained bodies (Fig. 2C). None of these cells had produced a polar body. Notably, we also found images of metaphase with only 10 DNA-stained bodies, which we interpret as being either figures of regular meiosis (~10% are expected) or the initial step of meiosis

I before abortion. From these results, we concluded that diploid oocytes in *M. belari* are formed after failure of the first anaphase of meiosis I. This modification will lead to the assortment of nonsister chromatids in the oocytes (equational division only). Such type of meiosis is often referred to as "central fusion automixis," because genetically, it corresponds to the fusion of the two first products of meiosis (Fig. 1A, d). In the presence of recombination for all chromosomes, this pattern of inheritance should progressively lead to LOH, distally to the crossover.

M. belari has a widely heterozygous genome

We analyzed the level and the distribution of heterozygosity in the genome of *M. belari* females, from our laboratory strain JU2817 and nine other wild strains, which had been sampled in different locations around the world (*17*). We sequenced mixed stage animals from each strain and mapped the short reads on the assembled genome of *M. belari* JU2817. We computed genome-wide heterozygosity by counting the proportion of heterozygous positions relative to the total number of positions using Analysis of Next Generation Sequencing Data (ANGSD) (*18*). Each strain being isofemale (see Materials and Methods), the genotype of a strain corresponds to the genotype of a single individual.

We found that all 10 strains had approximately the same level of heterozygosity of about 1.3% (SD = 0.2) (i.e., one residue every 75 nucleotides is heterozygous), demonstrating that the strains behaved similarly in the wild and in the laboratory (fig. S1 and table S1). This level of heterozygosity is unexpectedly high for a meiotic asexual experiencing regular recombination; it is 10 times higher than the self-fertilizing nematode *C. elegans* (*19*) and similar to natural populations of the fruit fly *Drosophila melanogaster* (*20*), for instance. Heterozygosity could be maintained in most parts of the chromosomes and lost only in subtelomeric regions if crossovers were restricted to chromosome ends, but we found that heterozygosity was uniform along all contigs (fig. S1). Analyzing this heterozygosity in the wild strains, we revealed the inbreeding coefficient F_{IS} being close to 0, i.e., $F_{IS} = 0.019$, throughout the genome. In a randomly mating species (Hardy-Weinberg expectation), F_{IS} equals 0. F_{IS} is negative if there is an excess of heterozygosity compared to the Hardy-Weinberg expectation, as found in asexuals that have lost recombination, via the so-called Meselson effect (*21*, *22*). F_{IS} is positive if there is a deficit of heterozygosity, as in selfers for instance (*23*). We had previously shown that out of 1000 females, no sexual females were produced (*13*). Such a F_{IS} value was therefore unexpected for a species with a rate of sexual reproduction close to 0 (Fig. 1A).

To further confirm the maintenance of heterozygosity, we performed a genome-wide analysis of genotype inheritance, from mother to daughters in *M. belari* JU2817. We performed this analysis on the transcriptome, which can be easily obtained from single worms. We analyzed three female individuals descended from the same mother. We mapped the RNA-sequencing (RNA-seq) reads to the previously assembled *M. belari* JU2817 transcriptome, and we called genotypes, focusing on sufficiently covered contigs and positions. Under the assumption of active recombination and random segregation of chromatids, large chromosomal segments—and therefore a substantial number of single-nucleotide polymorphisms (SNPs) and contigs—are expected to be homozygous in some of the females (Table 1). In contrast to this prediction, we found only a small minority of SNPs for which at least one daughter had a homozygous genotype (Table 1). These SNPs were most often surrounded by SNPs for which all three daughters were heterozygous, suggesting that there was no real stretch of homozygosity in any female. Among the >3200 contigs with more than two SNPs, only 9 contigs carried >2 SNPs homozygous in the same daughter. We found similar proportions when we performed the same analysis in another auto-pseudogamous species, *Mesorhabditis monhystera*. As a control, we also analyzed two sexual *Mesorhabditis* species *M. longespiculosa* and *M. spiculigera*. In these species, we found a large fraction of SNPs with homozygous genotypes (Table 1), as expected under random mating of gametes, with 737 (out of 1423, ~52%) and 1371 (out of 2953, ~46%) contigs, respectively, carrying >2 SNPs homozygous in the same daughter. This analysis indicates that the modified meiosis in auto-pseudogamous species of *Mesorhabditis* could fully preserve heterozygosity, from one generation to the next, and in the population overtime.

These results seem to contradict our initial cytological observations. We therefore determined whether despite the presence of structures that resemble chiasmata, homologous recombination might be absent, which would then explain the maintenance of heterozygosity in the short and long term upon assortment of nonsister chromatids.

Homologous chromosomes recombine during female meiosis

We wished to directly visualize crossovers as a formal proof that homologous recombination occurs during *M. belari* female meiosis. To this end, we used the thymidine analog 5-ethynyl-2′-deoxyuridine (EdU), which is incorporated into replicating DNA and can be fluorescently labeled. *M. belari* females were bathed in EdU (pulse phase) and then allowed to recover (chase phase) so that germ cells entered mitotic cycles with EdU and next divided and replicated without EdU. We optimized the pulse and chase periods to obtain chromosomes harboring only one EdU-labeled chromatid (fig. S2). Upon recombination, we then expected a strain exchange between one EdU-labeled (shown in pink) and one non–EdU-labeled chromatid (shown in blue, labeled only with Hoechst) in 50% of cases, generating bicolor chromatids (blue/pink) (Fig. 3 and fig. S2). We first analyzed the color of chromatids in diakinesis oocytes in which homologous chromosomes form chiasmata, i.e., bivalents. The expected figures of crossover in holocentric chromosomes has been described in (*24*) and is depicted in Fig. 3A. From eight oocytes, we identified 26 bivalent chromosomes whose orientation allowed us to unambiguously distinguish the chromatids within the chiasma. For 12 of them, the two opposed chromatids had the same color and could not be analyzed. Among the 14 showing opposed chromatids of different colors, 13 bivalents showed an exchange of chromatids, and only 1 showed no exchange (Fig. 3A). We also analyzed chromosomes in the female pronuclei of pseudogamous eggs during the first or second cell cycle, when chromosomes are condensed and chromatids are clearly visible. Cycles of DNA replication and mitosis had occurred in the absence of EdU in embryos, generating many chromatids devoid of EdU. Nevertheless, we counted 49 bicolor chromatids from 12 embryos (one representative embryo is shown in Fig. 3B). This analysis also revealed that chromatid exchange is not restricted to chromosome ends, as many chromosomes show large portions of EdU-positive chromatids (Fig. 3B). These results demonstrate that exchanges of strands between homologous chromosomes during meiosis are frequent

Table 1. Patterns of shared heterozygosity among sisters in four species of *Mesorhabditis*.

	Pseudogamous	Pseudogamous	Sexual	Sexual
Species	*M. belari*	*M. monhystera*	*M. spiculigera*	*M. longespiculosa*
No. of contigs	8381	8632	7099	7564
Mean coverage	37×	28×	42×	40×
No. of polymorphic sites	34,867	29,664	43,543	20,243
One-heterozygote*	1.44%	0.42%	45.3%	23.5%
Two-heterozygote†	0.89%	0.99%	22.1%	27.6%
Three-heterozygote‡	97.5%	98.5%	22.4%	39.4%
Other§	0.1%	0.06%	10.2%	9.5%

*Proportion of polymorphic sites at which exactly one of the three sisters was heterozygous. †Proportion of polymorphic sites at which exactly two of the three sisters were heterozygous. ‡Proportion of polymorphic sites at which all three sisters were heterozygous. §No heterozygote or unexpected allele call.

and that recombination, not restricted to telomeric regions, does occur in *M. belari* during the production of unreduced oocytes.

As another evidence that recombination is maintained in *M. belari*, we analyzed patterns of linkage disequilibrium (LD) across loci. In the absence of sex and recombination, alleles are expected to be strongly associated among loci, with haplotype blocks extending over long stretches of DNA. Recombination, if at work, breaks allele associations, leading to a decay of LD as the physical distance between SNPs increases (*25*). To assess the extent of LD in *M. belari*, we analyzed the genomic data previously obtained from the 10 strains. We called SNPs and used the LDhelmet program to estimate the genome-wide distribution of the effective population recombination rate ρ. This analysis indicated that, in both species, the estimated ρ was homogeneous across the genome with no local enrichment or losses (fig. S1), with a point estimate of the average ρ of 0.038 per base pair (bp). This implies that LD is lost as the distance between the considered loci exceeds ~100 bp. The average estimated ρ in *M. belari* was similar to estimates reported in sexual species of arthropods, such as *D. melanogaster* (*20*), and indicative of a high effective population recombination rate in this auto-pseudogamous species.

Chromatid segregation is biased during the unique meiotic division of *M. belari* embryos

Our cytological and genomic data are contradictory because recombination and random assortment of nonsister chromatids should lead to LOH. We reasoned that maintenance of heterozygosity from mother to daughters, and at the population level, can be achieved despite recombination, if either the two recombinants or the two nonrecombinant chromatids of a given chromosome pair cosegregate into the egg during the unique division of meiosis. We validated this hypothesis using our EdU experiment. Because *M. belari* chromosomes cannot be distinguished cytologically (i.e., pairs cannot be recognized), we used a statistical approach. We reasoned that under the hypothesis of cosegregating recombinant chromatids, we should always find an even number of recombinant chromatids in the nuclei of one-cell stage embryos, before the first mitosis. We reanalyzed another set of one-cell embryos, selecting only those in which chromosomes were well spread out at prometaphase so that chromosome axis was unambiguously identified. In the 11 embryos analyzed, we always found an even number of bicolor chromatids, ranging from 4 to 8 (Fig. 3C and fig. S3). Such a pattern would be obtained very rarely in the case of random segregation of the 20 chromatids (P value = 0.00048, binomial test, $n = 11$, $P = 0.5$). This result strongly supported that the single meiotic division of *M. belari* females is unique, as it leads to the cosegregation of recombinant chromatids (CRC).

Modeling the reproductive strategy of *M. belari* and the cosegregation of recombinant chromatids during meiosis

To assess whether CRC could reconcile cytological and genomic data, we developed a population genetics model. As output parameters, we considered the level of heterozygosity, the LD (as measured above), and the inbreeding coefficient F_{IS}.

We modeled the life cycle of *M. belari*, including the production of sexual males and asexual females with a biased sex ratio, the inbreeding mating structure [brother-sister mating or strong family structure as proposed by Grosmaire *et al.* (*13*)], and the modified meiosis with variable rate of LOH due to variable bias in the segregation of chromatids (Fig. 4, A and B). We also allowed for rare production of sexual females (i.e., being produced after mixing of the parental genomes). Although no sexual females have been observed under laboratory conditions, they may exist at low rate in natural populations, and it is an intermediate stage that necessarily occurred in the transition from sexuality to asexuality. We looked for conditions that could explain the observed genomic pattern: high heterozygosity, $F_{IS} \sim 0$, and low LD.

First, analytical results and multilocus simulations confirmed that CRC is needed to explain the absence of LOH. Second, considering deleterious mutations throughout the genome broadens the conditions that can explain the observed genomic patterns: Strict CRC is not required and sexual females can be produced at low rate (Fig. 4C and Supplementary Text). Actually, the production of sexual females at a very low rate better explains the low and flat LD pattern, as well as the $F_{IS} \sim 0$ than pure asexuality (Supplementary Text). The comparison of results without and with deleterious mutations also illustrates the central role that recessive deleterious mutations likely play in the system. Highly homozygous individuals that should be produced by imperfect CRC or leaky sex (that should lead to $F_{IS} > 0$; Fig. 4C neutral) are selected against, maintaining F_{IS} close to zero for a large range of conditions (Fig. 4C, with deleterious mutations). This also supports the idea that LOH should be

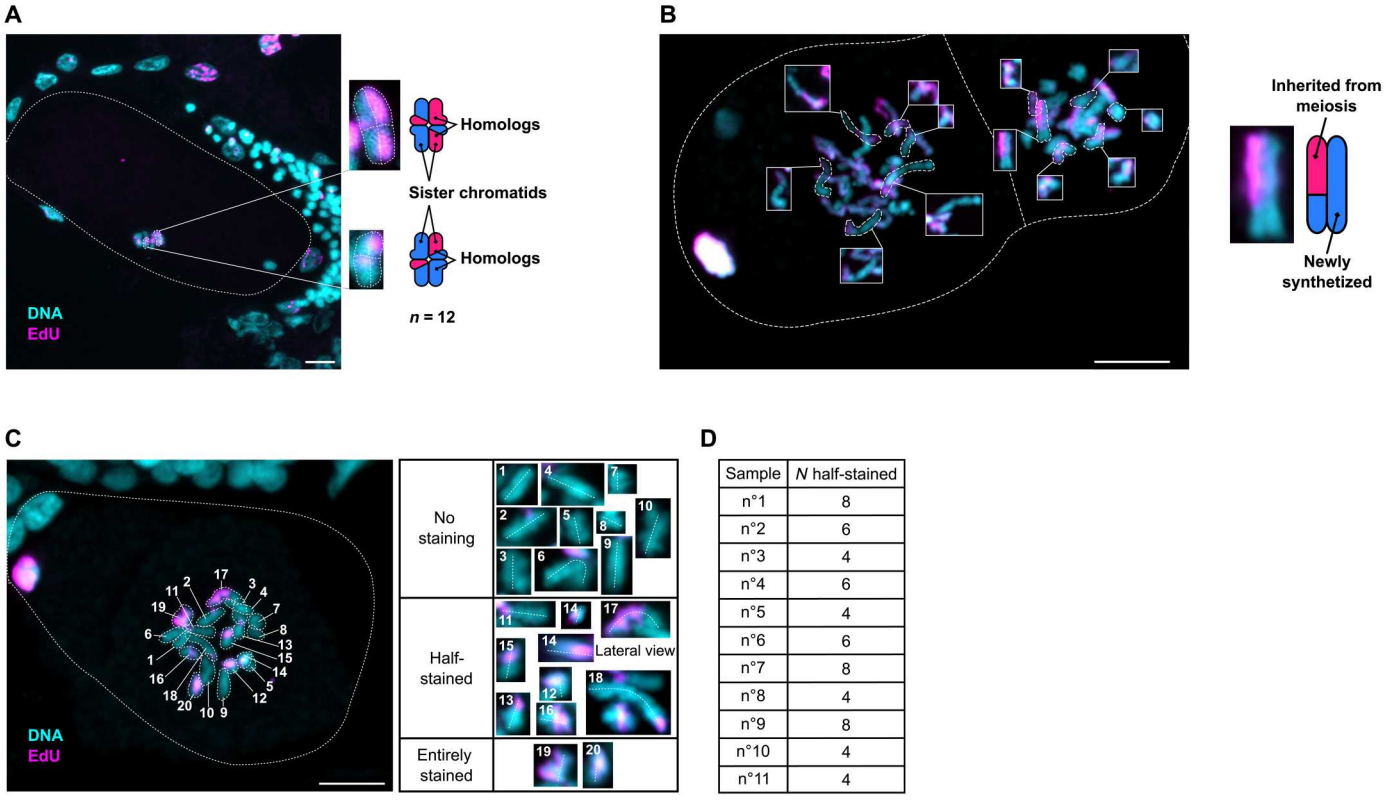

Fig. 3. Evidence of recombination and cosegregation of recombinant chromatids. Fixed embryos after an EdU experiment, where one chromatid out of the two is stained with EdU (in pink). DNA is in blue. Scale bar, 5 μm. (**A**) Embryo in metaphase of meiosis I (i.e., no polar body has been extruded yet). The metaphase plate is perpendicular to the glass slide. Few chromosomes are visible on this lateral view. The expected exchange of chromatids, as described in (*24*), is shown as well as the actual images in the inset. (**B**) Two-cell stage embryo during prometaphase. Most chromosomes have a bicolor chromatid (half-blue/half-pink, demonstrating recombination) and an unlabeled chromatid because it has replicated during the previous S phase in the absence of EdU (entirely blue). (**C**) One representative one-cell embryo in prometaphase. All 20 chromosomes are shown in the insets. Eight chromosomes are bicolor (#14 is shown twice). In (B) and (C), the polar body is visible on the left and contains EdU-labeled chromatids, as expected. (**D**) Table summarizing the count of recombinant chromatids from 11 embryos (also shown in fig. S3).

costly and suggests that CRC could be selected as a LOH-preventing mechanism.

We tested this hypothesis via a modification of the initial model whereby CRC can evolve. We first simulated a sexual species with random chromatid segregation at meiosis and added a locus controlling the proportion of asexual females produced (Fig. 4D, left). We assumed one mandatory crossover per chromosome. Hence, the asexual females experienced LOH with associated fitness reduction due to the expression of recessive deleterious mutations in homozygotes, a form of inbreeding depression. If inbreeding depression was higher than 0.5, it compensated for the advantage of not producing males and pseudogamy could not evolve. If inbreeding depression was lower than 0.5, pseudogamy rapidly evolved. Next, we introduced mutations at a second locus controlling CRC during asexual meiosis (in both directions: recombinants could be more positively or more negatively associated than at random) (Fig. 4D, right). We found that mutations leading to positive association between recombinants were selected for and that the population rapidly evolved toward complete CRC, preventing the deleterious effects of LOH. We also found that when mutations affecting pseudogamy and CRC were introduced at the same time, the two mechanisms co-evolved, speeding up and broadening the conditions for the evolution of pseudogamy (Fig. 4D and Supplementary Text). On the one hand, the occurrence of some asexual females enabled the evolution of CRC. On the other hand, once CRC started to evolve, it partly prevented the deleterious effect of LOH, further favoring the evolution of pseudogamy, even when inbreeding depression was higher than 0.5 (Fig. 4D). Our modeling approach thus confirmed that all a priori contradictory observations can be reconciled with the mechanism of CRC during the unique meiotic division of females, and our model provides a selective explanation for the evolution of such a peculiar mechanism from a sexual ancestor.

DISCUSSION

In this study, we found that *M. belari* asexual females are produced in the presence of recombination and assortment of nonsister chromatids, which should lead to rapid LOH, distally to the crossover. Our genomic analysis, however, revealed an unexpectedly high level of heterozygosity throughout the genome and no sign of LOH, even locally. Using a combination of cytological, genomic, and modeling approaches, we demonstrated that this pattern is possible provided the recombinant chromatids of each chromosome pair are not randomly assorted but instead cosegregate during the unique meiotic division. We named this type of non-Mendelian inheritance CRC.

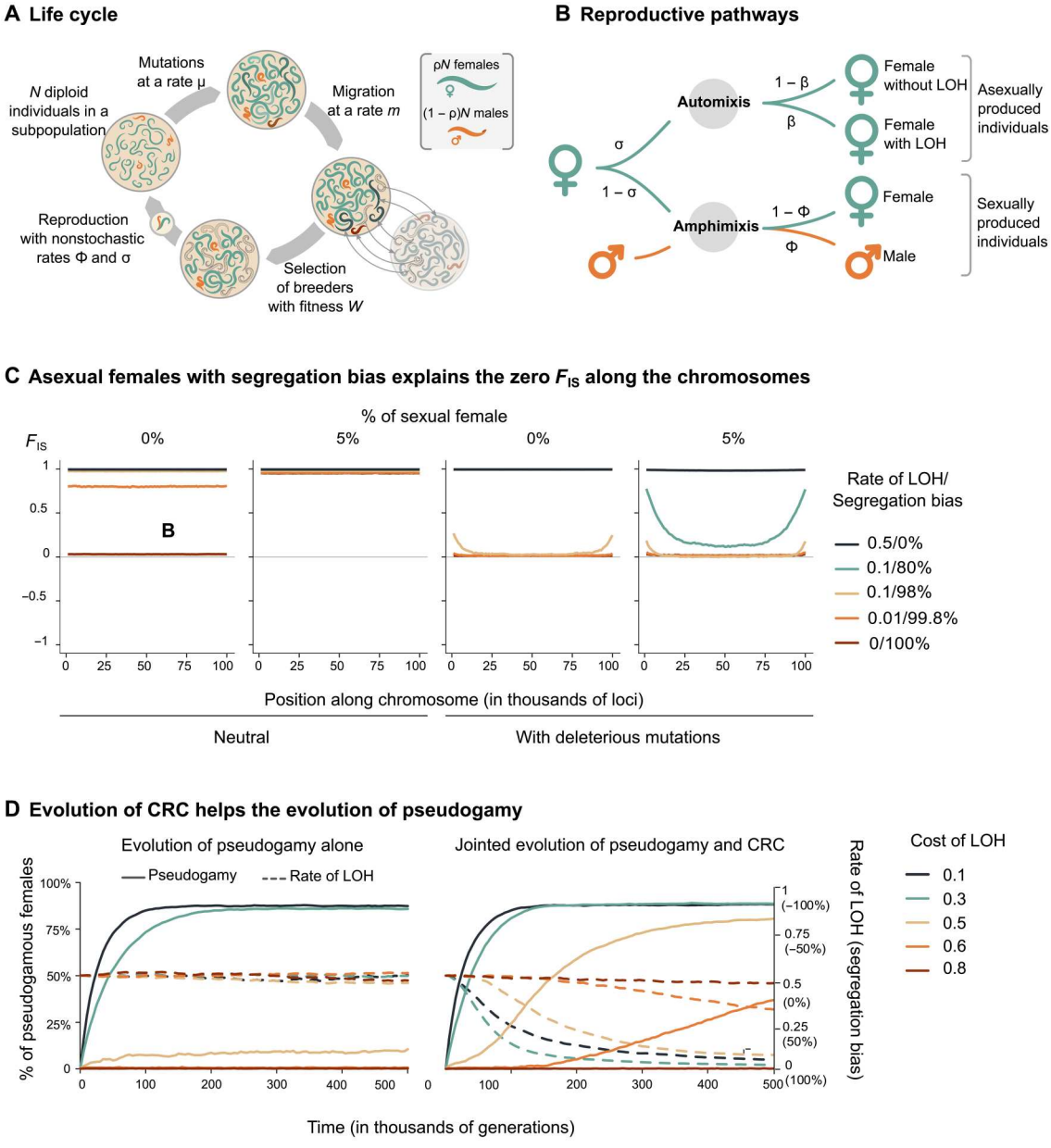

Fig. 4. Modeling the genomic consequences and evolution of CRC in *M. belari*. (**A**) Simulated life cycle with associated parameters. The generations are discrete and nonoverlapping, and we assume an island model to simulate the high level of consanguineous mating: The lower the local population size (N) and the migration rate (m), the higher the level of consanguineous mating. (**B**) Reproduction occurs either by automixis (i.e., producing asexual females) at rate σ or by amphimixis at rate 1 − σ. During automixis, the rate of LOH is β. With b, the cosegregation bias of recombinant chromatids, $\beta = \frac{1}{2}(1 - b)$. With no bias ($b = 0$) (i.e., random association of chromatids), β = ½, whereas with a full segregation bias ($b = 1$), there is no LOH. Note that complete LOH, β = 1, corresponds to negative cosegregation, when one recombinant always segregates with one nonrecombinant chromatid. Under sexual reproduction, females are produced at rate ϕ. ϕ is close to zero in natural populations. σ and ϕ determines the sex ratio, ρ. (**C**) F_{IS} along a chromosome as a function of the segregation bias and corresponding LOH, with or without sexually produced females and deleterious mutations. The total population size is 1000, and the migration rate is m = 0.0005. (**D**) Evolution of pseudogamy from an initially sexual population with different costs of LOH when the rate of LOH is fixed (β = ½), or when it is allowed to evolve through CRC. We assume 10% of males as in natural populations. Allowing the sex ratio to evolve does not change the result. The proportion of pseudogamous females (plain lines) reaches 90% when there are no more sexual females. The corresponding rate of LOH/segregation bias evolving with CRC is shown with dashed lines. Note that mutants increasing LOH (through a negative bias) are introduced in the simulations but are never selected for.

With CRC, specific pairs of chromatids are chosen during cell division such that the whole set of maternal alleles is transmitted to offspring (Fig. 5).

During their reproductive lifetime, *M. belari* females produce 10% reduced oocytes via regular meiotic divisions, which develop into sexual males, males being essential for sperm-dependent parthenogenesis (*13*). Hence, the meiotic program is intact in this species. This is a constraint for the evolution of asexuality because upon recombination, asexual females should experience LOH. We discovered CRC as an unexpected mechanism of LOH avoidance despite recombination.

How did CRC emerge during the evolution of auto-pseudogamy in *Mesorhabditis*? One hypothesis is that, initially, some females were produced sexually (i.e., after mixing of the parental genomes) when an X-bearing sperm fertilized the oocytes. Some females were also produced asexually through pseudogamy, after abortion of meiosis I but without CRC. In this context, asexual females experienced LOH, but this was compensated by the heterozygosity of sexual females. Once CRC appeared, LOH was prevented in the asexuals, next allowing the loss of most sexual females. Alternatively, a single modification of the meiotic program could have simultaneously generated a defect in anaphase I and a biased segregation of chromatids, immediately establishing asexual females without LOH.

At this stage, it is difficult to speculate on the molecular mechanism involved, and on a sequence of events, because, to our knowledge, no such phenotype has been described in mutants of model species. Nevertheless, we hypothesize that failure of joint molecule resolution during crossover could maintain the two recombinant chromatids physically attached. Consequently, this attachment would prevent the correct segregation of bivalents during meiosis I. Several nucleases involved in crossover resolution, such as MUS-81 and SLX-4 of XPF-1 (*26*, *27*) or LEM-3/Ankle1, which eliminates the persistent DNA linkages during meiotic II in *C. elegans* (*28*), could be involved. We hypothesize that some of these factors could be down-regulated or have a delayed activity in the oocytes experiencing an incomplete meiotic division in *M. belari*. In contradiction with this hypothesis, we have not been able to detect DNA threads between the separating chromosomes. However, thin DNA threads are most often not detectable with conventional DNA staining as we have used in this study but only with immunofluorescent staining for proteins that bind these threads (*29*). A systematic analysis of the dynamic localization of the nucleases involved in crossover resolution in *M. belari* may help determine whether or not a persisting physical link is responsible for CRC. An alternative hypothesis is that despite proper crossover resolution and loss of a physical attachment, some of the proteins that are differentially loaded on chromatids during meiotic prophase remain specifically attached to the recombinant chromatids. Such "tagging" could contribute to a directed rotation of chromatids during meiosis II, with recombinant facing the same pole of the spindle. Exploration of *M. belari* mutants affecting the different steps of crossover establishment and resolution will be necessary to shed light on the mechanisms at the origin of CRC.

Another mechanism of LOH avoidance has been previously proposed for recombining asexuals, which relies on distal crossover location (*6*, *30*). However, distal crossovers are very unstable for the *C. elegans* holocentric chromosomes and often lead to aneuploidy (*31*), suggesting that such mechanism of LOH avoidance could not have been selected in a holocentric species such as *M. belari*. Another mechanism involving inverted meiosis (which is compatible with holocentricity), failed meiosis II, and biased chromatid segregation has been proposed for the maintenance of heterozygosity in the asexual oribatid mites (*32*, *33*). Although such biased segregation of chromatids remains hypothetical in the absence of further cytological description, it is conceptually similar to the CRC we describe in our study.

If distal COs are most likely not compatible with holocentric species, can CRC evolve as a mechanism of LOH avoidance in asexual species with monocentric chromosomes? We suspect that CRC is not necessarily restricted to holocentric species. In holocentric chromosomes, the CO serves as a focal point to establish the chromosome subdomains, necessary for the sequential dissociation of cohesins and, hence, chromatids (*34*). Therefore, even in the absence of a single centromere, the same principles of chromosome organization and dissociation hold in monocentric and holocentric species. Consequently, co-orientation of recombinant chromatids could also be at play in monocentric species. However, in species that establish multiple crossovers between all chromatids within a pair of homologs (*35*), which is restricted to monocentric species,

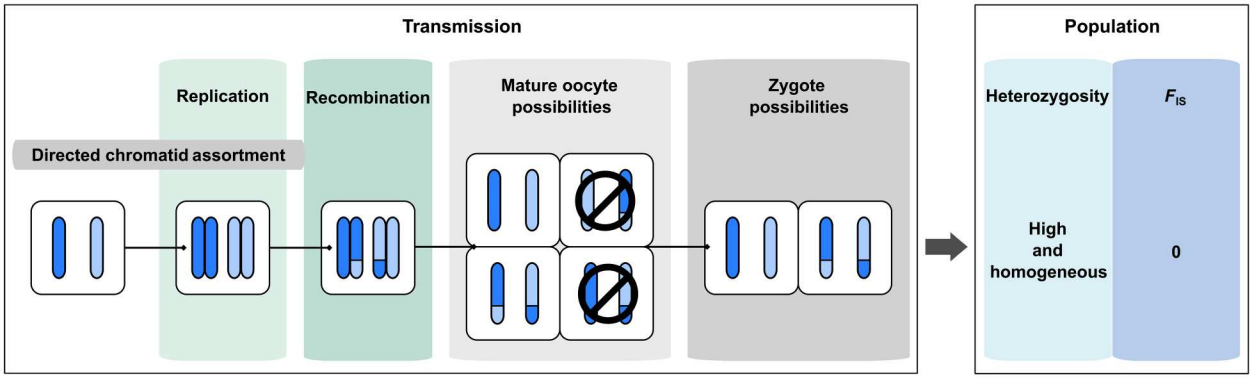

Fig. 5. Mechanism of heterozygosity maintenance via CRC in *M. belari*. Schematic representation of meiosis and CRC during the production of diploid oocytes in *M. belari*. Homologous chromosomes (in blue) are initially heterozygous in the mother (shown in nuances of blue). After recombination and failure of meiosis I, nonsister chromatids do not segregate randomly during meiosis II. Instead, cosegregation of recombinant chromatids maintains heterozygosity in the progeny and in the population.

there will be no possibility to cosegregate the recombinants together. Hence, CRC can probably emerge only in species that initially have a limited number of crossovers per chromosome, as previously proposed (*6*), or at least multiple crossovers restricted to a single pair of chromatids.

Although different from CRC, evidence of biased segregation of recombinant chromatids already exists in monocentric species. For instance, in *Drosophila*, during mitotic recombination, the recombinant chromatids of a given pair of chromosomes systematically segregate away in the daughter cells, which is the opposite to the CRC bias (*36*). In human oocytes, after the two regular steps of meiosis, the recombinant chromatids are preferentially inherited in the oocytes (*37*). Here as well, the mechanisms behind the segregation bias remain to be determined, but together with CRC, these examples show that recombinant and nonrecombinant chromatids can be sorted out during cell divisions.

Last, most asexual animal models have been characterized either by cytology or by genomics, rarely both, whereas such a combination of approaches was decisive here. In most cases, the level of recombination in the asexual lineages was inferred from the observed rate of LOH. For the Cape honey bee, the crustaceans *Artemia parthenogenetica* and *Daphnia magna* or the ant *Cerapachys biroi* to only cite a few, a reduction in the rate of recombination has been invoked to account for the observed level of elevated heterozygosity and absence of LOH (*6*, *30*, *38*, *39*). In the light of our discovery in *M. belari*, we would like to propose CRC as a possible alternative explanation. Overall, there is an exciting possibility that CRC has been selected multiple times independently in the evolution of asexuals, as an efficient strategy against the detrimental effect of LOH.

MATERIALS AND MEHODS

Nematode strains and culture

Mesorhabditis species are maintained at 20°C on Nematode Growth Media (NGM) plates seeded with *Escherichia coli* OP50, following *C. elegans* protocols, as described in (*13*).

Immunostainings on gonads and embryos

We performed immunostainings as described in (*13*). We dissected gravid females on slides coated with 0.25% poly-lysine in 0.5× M9. After freeze cracking, we fixed the samples by immersing slides into methanol at −20°C for at least 5 min. We used a mouse anti-tubulin antibody as primary antibody (1:2000; Sigma-Aldrich, DM1A) and an Alexa Fluor 488 donkey anti-mouse secondary antibody (1:2000; Jackson ImmunoResearch, #715-545-150). We incubated both antibodies at room temperature for 45 min. DNA was stained using Hoechst 33258 at 0.5 μl/ml (Merck Sigma-Aldrich, #94403). Images were acquired using a confocal microscope (oil immersion 63× objective, LSM800 and LSM980 Airyscan, Zeiss). *Z*-stacks of embryos were acquired every 0.15 μm. Last, we treated the acquired images using the ImageJ 1.53t software.

EdU pulse/chase protocol

We adapted the protocol from (*15*). To obtain diakinesis oocytes and early embryos for which only one chromatid per chromosome was labeled with EdU, we had to optimize the protocol for *M. belari*. First, we synchronized worms using axenization, as described in (*13*). Briefly, we collected worms and treated them with bleach and NaOH to dissolve all individuals except the embryos. We washed the embryo pellet and placed it on plates without bacteria, allowing L1 larvae to hatch. Without food, all L1s were arrested at the same stage after 2 days. We placed L1s back on food and allowed them to grow for 72 hours at 20°C. At this stage, we collected the young L4 synchronized worms and washed them in 1× phosphate-buffered saline (PBS) and 0.1% Triton X-100. We transferred a pellet of ~300 μl of worms into 200 μl of 10 mM EdU diluted in water (Thermo Fisher Scientific, A10044) to obtain a final concentration of 4 mM EdU. We transferred the tube on a rotator for 4 hours at room temperature. After washes in M9, we plated the animals onto fresh NGM plates seeded with *E. coli* and placed them at 25°C for 48 hours before embryos were collected for fixation. As summarized in fig. S2, we deduced that two rounds of S phase precede meiotic prophase during *M. belari* oogenesis.

EdU click-it labeling

Cytology was performed following the instructions provided by the EdU Click-it kit (Thermo Fisher Scientific, C10337). We collected the embryos after axenization, as described above. We placed the embryos on poly-lysine–coated slides and freeze-cracked and fixed them in −20°C methanol. We incubated the samples with bovine serum albumin 2% for 20 min at room temperature. We washed the slides twice with 1× PBS. Following the instructions of the kit, we washed the slides for 30 min at room temperature in 1× PBS with 1% Triton X-100 (v/v) and labeled them with Alexa Fluor 488–azide for 30 min at room temperature. We washed the samples twice with 1× PBS and incubated them in a tank with Hoechst 33258 for 20 min at room temperature. Last, we mounted the slides using ProLong Diamond Antifade Mountant (Thermo Fisher Scientific, P36965) and sealed them with nail polish. For scoring the segregation of recombinant chromatids, we first screened the slides for one-cell stage embryos in prometaphase, because at this stage, the chromosomes are well condensed and the chromatids can be easily visualized. Among these embryos, we first selected the embryos for which the EdU signal is present on the DNA but is not uniform (which happens if the EdU was present during too many S phases). Second, we scored only those embryos for which the 20 chromosomes were nicely spread, to be confident about the color of the chromatids. For this reason, the number of analyzed embryos remains limited. This is a technical limitation of the study system because with these nematode embryos, we cannot synchronize the embryos to increase the number of cells in prometaphase and we cannot perform metaphase spread because of the eggshell surrounding the cells.

Airyscan and ImageJ 3D analysis of EdU-labeled recombinant chromatids

As with immunostaining, confocal airyscan images were acquired using the Zeiss LSM800 Airyscan and LSM980 Airyscan using a 63× oil objective and a 0.15-μm interval between slides. Images were subsequently processed by the airyscan processing method [three-dimensional (3D) analysis, automatic low stringency, Zen Blue 3.3]. Processed images were treated using ImageJ 1.53t software. Analyses of each chromosome were done using a combination of Z projection and 3D projection on the *y* axis using the brightest point method and interpolation.

DNA and RNA preparation for sequencing

We performed DNA sequencing on 10 strains of the auto-pseudogamous species *M. belari* coming from different locations in Europe (accession numbers PRJEB30104 and PRJEB61636). For each strain, one gravid female was initially collected in the wild and left to lay eggs in a Petri dish. This constituted a single strain, which was frozen in our collection. For sequencing, we amplified the animals and extracted the DNA for each strain. Briefly, we collected mixed stage worms, washed them in M9, and we froze a pellet of ~300 µl of worms in liquid nitrogen. After thawing, we added 600 µl of cell lysis buffer (Qiagen Cell Lysis Solution, #158906), as well as 6 µl of proteinase K at 17 µg/µl and incubated the mix for 3 hours at 65°C. We next incubated the mix for 1 hour at 37°C, supplemented with 40 µl of ribonuclease A (at 5 mg/ml). We added 200 µl of protein precipitation solution (Qiagen, #158912), and after 5 min on ice, we centrifuged the mix for 10 min at 13,000 rpm at 4°C. We next added 600 µl of isopropanol to the supernatant. After 10 min at room temperature, we centrifuged the mix at maximum speed, and we rinsed the pellet twice in ethanol 70°C. We then dried the pellet, and resuspended it in nuclease-free water.

For the analysis of genotype inheritance in sisters, we isolated gravid females, for each species, let them lay eggs, and, after few days, isolated three virgin daughters. We extracted the mRNAs of each single female using the SmartSeq2 protocol, as described in (*40*). For all samples, we prepared genomic libraries (insert sizes of ~550 bp) using TruSeqNano, and we sequenced the libraries on a HiSeq4000 with 100-bp paired-end read length.

Heterozygosity analysis

For each of the 10 strains of *M. belari*, we mapped the reads to the assembled genome of *M. belari* (accession number PRJEB30104) with BWA (Burrow-Wheeler Aligner) (*41*). The assembled genome is still fragmented, containing 217 contigs. We therefore analyzed heterozygosity along all 217 contigs (see fig. S1 and zenodo archive; https://doi.org/10.5281/zenodo.8112093). We produced BAM files with SAMtools (*42*), and we estimated the heterozygosity for each strain using ANGSD (*18*) using the Site Frequency Spectrum (SFS) estimation for a single sample. Recombination at the extremities of the chromosomes could explain a limited decrease in heterozygosity, with the rest of the chromosome remaining non-recombining. To test this, we calculated the heterozygosity on 5000-bp windows. A decrease in heterozygosity at the ends of the contigs was then looked for, graphically. At first, we detected homozygous portions in the JU2817 strain. However, these portions were twice as low in coverage as the rest of the contigs, which could be explained by an assembly error due to too much divergence between the two alleles. A similarity search with blastn allowed us to detect the presence of indels between the two alleles, preventing a unique assembly of these regions. We did not find this pattern in the other strains and therefore explains the lower heterozygosity of this strain compared to the others (i.e., haplotype divergence).

Genotype inheritance

RNA-seq was performed for three sisters in each of the two auto-pseudogamous species *M. belari* and *M. monhystera* and the two sexual species *M. spiculigera* and *M. longespiculosa* (accession number PRJEB61636). For each species, reads from the three individuals where pooled to assemble a transcriptome: Adapters were clipped from the sequences, low-quality read ends were trimmed (phred score < 30), and low-quality reads were discarded (remaining length <36 bp) using trimmomatic [v0.39; (*43*)]. Paired-end transcriptomes were de novo assembled using Trinity v2.13.2 (*44*). We mapped the reads on their respective assembled transcriptome with BWA (*41*), and we produced the BAM files with SAMtools (*42*) and called the SNPs using reads2SNP (*45*) focusing on sufficiently covered contigs (minimum contig average coverage = 15×) and positions (minimum = 20×). In each species, we selected positions in which not only the called genotypes but also read frequencies varied significantly among sisters. Specifically, for each position, two multinomial models were fitted to read counts. Model M0 (three degrees of freedom) assumed a common frequency of A, C, G, and T in the three sisters. Model M1 (9 degrees of freedom) rather allowed each of the three sisters to have its own frequencies of A, C, G, and T reads. We performed a likelihood ratio test, and we analyzed only positions in which M0 was rejected ($P < 1.0 \times 10^{-8}$). This was intended to exclude positions for which the genotype varied among sisters due to uncertainty in genotype calling.

Measure of LD

To test for the existence of recombination, we estimated the LD using the 10 strains of *M. belari*. For each of the 10 strains, we mapped the reads to the assembled genome with BWA (*41*). We produced BAM files with SAMtools (*42*), and we called the SNPs with reads2SNP (*45*). To phase haplotypes, we first used WhatsHap (*46*) to extract the phase information contained in reads. We completed phasing using Beagle v5.3 (*47*). We computed LD on 5000-bp windows with LDhelmet v1.10 (*20*) using recommended parameters.

Supplementary Materials

This PDF file includes:

Figs. S1 to S9
Table S1
Supplementary text
Legends for data S1 to S3
References

Other Supplementary Material for this manuscript includes the following:

Data S1 to S3

REFERENCES AND NOTES

1. E. Suomalainen, A. Saura, J. Lokki, *Cytology and Evolution in Parthenogenesis* (CRC Press, 1987).
2. M. Neiman, T. F. Sharbel, T. Schwander, Genetic causes of transitions from sexual reproduction to asexuality in plants and animals. *J. Evol. Biol.* **27**, 1346–1359 (2014).
3. T. Lenormand, J. Engelstädter, S. E. Johnston, E. Wijnker, C. R. Haag, Evolutionary mysteries in meiosis. *Philos. Trans. R. Soc. Lond. B Biol. Sci.* **371**, 20160001 (2016).
4. M. Archetti, Complementation, genetic conflict, and the evolution of sex and recombination. *J. Hered.* **101**, S21–S33 (2010).
5. J. Engelstädter, Constraints on the evolution of asexual reproduction. *Bioessays* **30**, 1138–1150 (2008).
6. C. R. Haag, L. Theodosiou, R. Zahab, T. Lenormand, Low recombination rates in sexual species and sex-asex transitions. *Philos. Trans. R. Soc. Lond. B Biol. Sci.* **372**, 20160461 (2017).
7. K. S. Jaron, J. Bast, R. W. Nowell, T. R. Ranallo-Benavidez, M. Robinson-Rechavi, T. Schwander, Genomic features of parthenogenetic animals. *J. Hered.* **112**, 19–33 (2021).
8. A. Brandt, P. Tran Van, C. Bluhm, Y. Anselmetti, Z. Dumas, E. Figuet, C. M. François, N. Galtier, B. Heimburger, K. S. Jaron, M. Labédan, M. Maraun, D. J. Parker, M. Robinson-Rechavi,

I. Schaefer, P. Simion, S. Scheu, T. Schwander, J. Bast, Haplotype divergence supports long-term asexuality in the oribatid mite *Oppiella nova*. *Proc. Natl. Acad. Sci. U.S.A.* **118**, e2101485118 (2021).
9. P. Simion, J. Narayan, A. Houtain, A. Derzelle, L. Baudry, E. Nicolas, R. Arora, M. Cariou, C. Cruaud, F. R. Gaudray, C. Gilbert, N. Guiglielmoni, B. Hespeels, D. K. L. Kozlowski, K. Labadie, A. Limasset, M. Llirós, M. Marbouty, M. Terwagne, J. Virgo, R. Cordaux, E. G. J. Danchin, B. Hallet, R. Koszul, T. Lenormand, J.-F. Flot, K. Van Doninck, Chromosome-level genome assembly reveals homologous chromosomes and recombination in asexual rotifer *Adineta vaga*. *Sci. Adv.* **7**, eabg4216 (2021).
10. P. Tran Van, Y. Anselmetti, J. Bast, Z. Dumas, N. Galtier, K. S. Jaron, K. Martens, D. J. Parker, M. Robinson-Rechavi, T. Schwander, P. Simion, I. Schön, First annotated draft genomes of nonmarine ostracods (Ostracoda, Crustacea) with different reproductive modes. *G3 (Bethesda)* **11**, jkab043 (2021).
11. H. Fradin, K. Kiontke, C. Zegar, M. Gutwein, J. Lucas, M. Kovtun, D. L. Corcoran, L. R. Baugh, D. H. A. Fitch, F. Piano, K. C. Gunsalus, Genome architecture and evolution of a unichromosomal asexual nematode. *Curr. Biol.* **27**, 2928–2939.e6 (2017).
12. R. Guidetti, M. Cesari, R. Bertolani, T. Altiero, L. Rebecchi, High diversity in species, reproductive modes and distribution within the *Paramacrobiotus richtersi* complex (Eutardigrada, Macrobiotidae). *Zool. Lett.* **5**, 1 (2019).
13. M. Grosmaire, C. Launay, M. Siegwald, T. Brugière, L. Estrada-Virrueta, D. Berger, C. Burny, L. Modolo, M. Blaxter, P. Meister, M.-A. Félix, P.-H. Gouyon, M. Delattre, Males as somatic investment in a parthenogenetic nematode. *Science* **363**, 1210–1213 (2019).
14. D. G. Albertson, J. N. Thomson, Segregation of holocentric chromosomes at meiosis in the nematode, *Caenorhabditis elegans*. *Chromosome Res.* **1**, 15–26 (1993).
15. D. E. Almanzar, S. G. Gordon, O. Rog, Meiotic sister chromatid exchanges are rare in *C. elegans*. *Curr. Biol.* **31**, 1499–1507.e3 (2021).
16. A.-C. Valfort, C. Launay, M. Sémon, M. Delattre, Evolution of mitotic spindle behavior during the first asymmetric embryonic division of nematodes. *PLOS Biol.* **16**, e2005099 (2018).
17. C. Launay, M.-A. Félix, J. Dieng, M. Delattre, Diversification and hybrid incompatibility in auto-pseudogamous species of *Mesorhabditis* nematodes. *BMC Evol. Biol.* **20**, 105 (2020).
18. T. S. Korneliussen, A. Albrechtsen, R. Nielsen, ANGSD: Analysis of next generation sequencing data. *BMC Bioinformatics* **15**, 356 (2014).
19. E. C. Andersen, J. P. Gerke, J. A. Shapiro, J. R. Crissman, R. Ghosh, J. S. Bloom, M.-A. Félix, L. Kruglyak, Chromosome-scale selective sweeps shape *Caenorhabditis elegans* genomic diversity. *Nat. Genet.* **44**, 285–290 (2012).
20. A. H. Chan, P. A. Jenkins, Y. S. Song, Genome-wide fine-scale recombination rate variation in *Drosophila melanogaster*. *PLOS Genet.* **8**, e1003090 (2012).
21. F. Balloux, L. Lehmann, T. de Meeûs, The population genetics of clonal and partially clonal diploids. *Genetics* **164**, 1635–1644 (2003).
22. S. L. Ament-Velásquez, E. Figuet, M. Ballenghien, E. E. Zattara, J. L. Norenburg, F. A. Fernández-Álvarez, J. Bierne, N. Bierne, N. Galtier, Population genomics of sexual and asexual lineages in fissiparous ribbon worms (Lineus, Nemertea): Hybridization, polyploidy and the Meselson effect. *Mol. Ecol.* **25**, 3356–3369 (2016).
23. S. Glémin, N. Galtier, Genome evolution in outcrossing versus selfing versus asexual species. *Methods Mol. Biol.* **855**, 311–335 (2012).
24. M. Mandrioli, G. C. Manicardi, Holocentric chromosomes. *PLOS Genet.* **16**, e1008918 (2020).
25. M. P. H. Stumpf, G. A. T. McVean, Estimating recombination rates from population-genetic data. *Nat. Rev. Genet.* **4**, 959–968 (2003).
26. A. Agostinho, B. Meier, R. Sonneville, M. Jagut, A. Woglar, J. Blow, V. Jantsch, A. Gartner, Combinatorial regulation of meiotic holliday junction resolution in *C. elegans* by HIM-6 (BLM) helicase, SLX-4, and the SLX-1, MUS-81 and XPF-1 nucleases. *PLOS Genet.* **9**, e1003591 (2013).
27. N. J. O'Neil, J. S. Martin, J. L. Youds, J. D. Ward, M. I. R. Petalcorin, A. M. Rose, S. J. Boulton, Joint molecule resolution requires the redundant activities of MUS-81 and XPF-1 during *Caenorhabditis elegans* meiosis. *PLOS Genet.* **9**, e1003582 (2013).
28. Y. Hong, M. Velkova, N. Silva, M. Jagut, V. Scheidt, K. Labib, V. Jantsch, A. Gartner, The conserved LEM-3/Ankle1 nuclease is involved in the combinatorial regulation of meiotic recombination repair and chromosome segregation in *Caenorhabditis elegans*. *PLOS Genet.* **14**, e1007453 (2018).
29. Y. Liu, C. F. Nielsen, Q. Yao, I. D. Hickson, The origins and processing of ultra fine anaphase DNA bridges. *Curr. Opin. Genet. Dev.* **26**, 1–5 (2014).
30. B. P. Oldroyd, B. Yagound, M. H. Allsopp, M. J. Holmes, G. Buchmann, A. Zayed, M. Beekman, Adaptive, caste-specific changes to recombination rates in a thelytokous honeybee population. *Proc. R. Soc. B Biol. Sci.* **288**, 20210729 (2021).
31. E. Altendorfer, L. I. Láscarez-Lagunas, S. Nadarajan, I. Mathieson, M. P. Colaiácovo, Crossover position drives chromosome remodeling for accurate meiotic chromosome segregation. *Curr. Biol.* **30**, 1329–1338.e7 (2020).
32. G. Taberly, The cytology of parthenogenesis in *Platynothrus peltifer* (Koch) (Acarien, Oribate). *C. R. Hebd. Seances Acad. Sci.* **247**, 1655–1657 (1958).
33. M. Archetti, Evidence from automixis with inverted meiosis for the maintenance of sex by loss of complementation. *J. Evol. Biol.* **35**, 40–50 (2022).
34. M. Schvarzstein, S. M. Wignall, A. M. Villeneuve, Coordinating cohesion, co-orientation, and congression during meiosis: Lessons from holocentric chromosomes. *Genes Dev.* **24**, 219–228 (2010).
35. M. Sarens, G. P. Copenhaver, N. De Storme, The role of chromatid interference in determining meiotic crossover patterns. *Front. Plant Sci.* **12**, 656691 (2021).
36. K. J. Beumer, S. Pimpinelli, K. G. Golic, Induced chromosomal exchange directs the segregation of recombinant chromatids in mitosis of *Drosophila*. *Genetics* **150**, 173–188 (1998).
37. C. S. Ottolini, L. Newnham, A. Capalbo, S. A. Natesan, H. A. Joshi, D. Cimadomo, D. K. Griffin, K. Sage, M. C. Summers, A. R. Thornhill, E. Housworth, A. D. Herbert, L. Rienzi, F. M. Ubaldi, A. H. Handyside, E. R. Hoffmann, Genome-wide maps of recombination and chromosome segregation in human oocytes and embryos show selection for maternal recombination rates. *Nat. Genet.* **47**, 727–735 (2015).
38. P. R. Oxley, L. Ji, I. Fetter-Pruneda, S. K. McKenzie, C. Li, H. Hu, G. Zhang, D. J. C. Kronauer, The genome of the clonal raider ant *Cerapachys biroi*. *Curr. Biol.* **24**, 451–458 (2014).
39. M. Dukić, D. Berner, C. R. Haag, D. Ebert, How clonal are clones? A quest for loss of heterozygosity during asexual reproduction in *Daphnia magna*. *J. Evol. Biol.* **32**, 619–628 (2019).
40. L. Serra, D. Z. Chang, M. Macchietto, K. Williams, R. Murad, D. Lu, A. R. Dillman, A. Mortazavi, Adapting the Smart-seq2 protocol for robust single worm RNA-seq. *Bio. Protoc.* **8**, e2729 (2018).
41. H. Li, R. Durbin, Fast and accurate short read alignment with Burrows-Wheeler transform. *Bioinformatics* **25**, 1754–1760 (2009).
42. H. Li, B. Handsaker, A. Wysoker, T. Fennell, J. Ruan, N. Homer, G. Marth, G. Abecasis, R. Durbin; 1000 Genome Project Data Processing Subgroup, The sequence alignment/map format and SAMtools. *Bioinformatics* **25**, 2078–2079 (2009).
43. A. M. Bolger, M. Lohse, B. Usadel, Trimmomatic: A flexible trimmer for Illumina sequence data. *Bioinformatics* **30**, 2114–2120 (2014).
44. M. G. Grabherr, B. J. Haas, M. Yassour, J. Z. Levin, D. A. Thompson, I. Amit, X. Adiconis, L. Fan, R. Raychowdhury, Q. Zeng, Z. Chen, E. Mauceli, N. Hacohen, A. Gnirke, N. Rhind, F. di Palma, B. W. Birren, C. Nusbaum, K. Lindblad-Toh, N. Friedman, A. Regev, Full-length transcriptome assembly from RNA-Seq data without a reference genome. *Nat. Biotechnol.* **29**, 644–652 (2011).
45. P. Gayral, J. Melo-Ferreira, S. Glémin, N. Bierne, M. Carneiro, B. Nabholz, J. M. Lourenco, P. C. Alves, M. Ballenghien, N. Faivre, K. Belkhir, V. Cahais, E. Loire, A. Bernard, N. Galtier, Reference-free population genomics from next-generation transcriptome data and the vertebrate-invertebrate gap. *PLOS Genet.* **9**, e1003457 (2013).
46. M. Patterson, T. Marschall, N. Pisanti, L. van Iersel, L. Stougie, G. W. Klau, A. Schönhuth, WhatsHap: Weighted haplotype assembly for future-generation sequencing reads. *J. Comput. Biol.* **22**, 498–509 (2015).
47. B. L. Browning, X. Tian, Y. Zhou, S. R. Browning, Fast two-stage phasing of large-scale sequence data. *Am. J. Hum. Genet.* **108**, 1880–1890 (2021).
48. J. Engelstädter, Asexual but not clonal: Evolutionary processes in automictic populations. *Genetics* **206**, 993–1009 (2017).
49. F. Prugnolle, T. De Meeus, Apparent high recombination rates in clonal parasitic organisms due to inappropriate sampling design. *Heredity* **104**, 135–140 (2010).
50. B. C. Haller, P. W. Messer, SLiM 3: Forward genetic simulations beyond the wright-fisher model. *Mol. Biol. Evol.* **36**, 632–637 (2019).
51. F. Rousset, *Genetic Structure and Selection in Subdivided Populations* (Princeton Univ. Press, 2004), vol. 40.
52. Wolfram-Research Inc., *Mathematica Edition: Version 8.0* (Wolfram Research, 2010).

Acknowledgments: We acknowledge the contribution of the imaging platform PLATIM from SFR Biosciences Lyon, as well as the sequencing platform Genomeast Strasbourg and the Institut de Genomique Fonctionnelle de Lyon (IGFL) sequencing platform. We also thank C. Rey for help with the treatment of the NGS raw data. We thank R. Dubruille and B. Loppin for critical reading of the manuscript. **Funding:** This work has been supported by a grant from the ANR-19-CE02-0012-01 to M.D., N.G., and S.G. and PhD fellowship from CNRS to C.B. **Author contributions:** M.D., N.G., and S.G. designed the experiments. S.G. designed the model. E.L.F. developed the simulation code, and ran and analyzed the simulations with L.M.-O. and S.G. C.D., N.S., and N.G. analyzed the genomic data. C.B., E.W., and M.D. performed the experimental work. C.B., N.S., N.G., S.G., and M.D. wrote the manuscript. **Competing interests:** The authors declare that they have no competing interests. **Data and materials availability:** All data needed to evaluate the conclusions in the paper are present in the paper and/or the Supplementary

Materials except data related to sequencing, which can be found on ebi.ac.uk/ena accession numbers PRJEB30104 and PRJEB36916.

Submitted 15 April 2023
Accepted 27 July 2023
Published 25 August 2023
10.1126/sciadv.adi2804

ScienceAdvances

Cosegregation of recombinant chromatids maintains genome-wide heterozygosity in an asexual nematode

Caroline Blanc, Nathanaelle Saclier, Ehouarn Le Faou, Lucas Marie-Orleach, Eva Wenger, Celian Diblasi, Sylvain Glemin, Nicolas Galtier, and Marie Delattre

Sci. Adv. **9** (34), eadi2804. DOI: 10.1126/sciadv.adi2804

Science Advances
AAAS

Supplementary Materials for

Cosegregation of recombinant chromatids maintains genome-wide heterozygosity in an asexual nematode

Caroline Blanc *et al.*

Corresponding author: Marie Delattre, marie.delattre@ens-lyon.fr

Sci. Adv. **9**, eadi2804 (2023)
DOI: 10.1126/sciadv.adi2804

The PDF file includes:

Other Supplementary Material for this manuscript includes the following:

Fig. S1

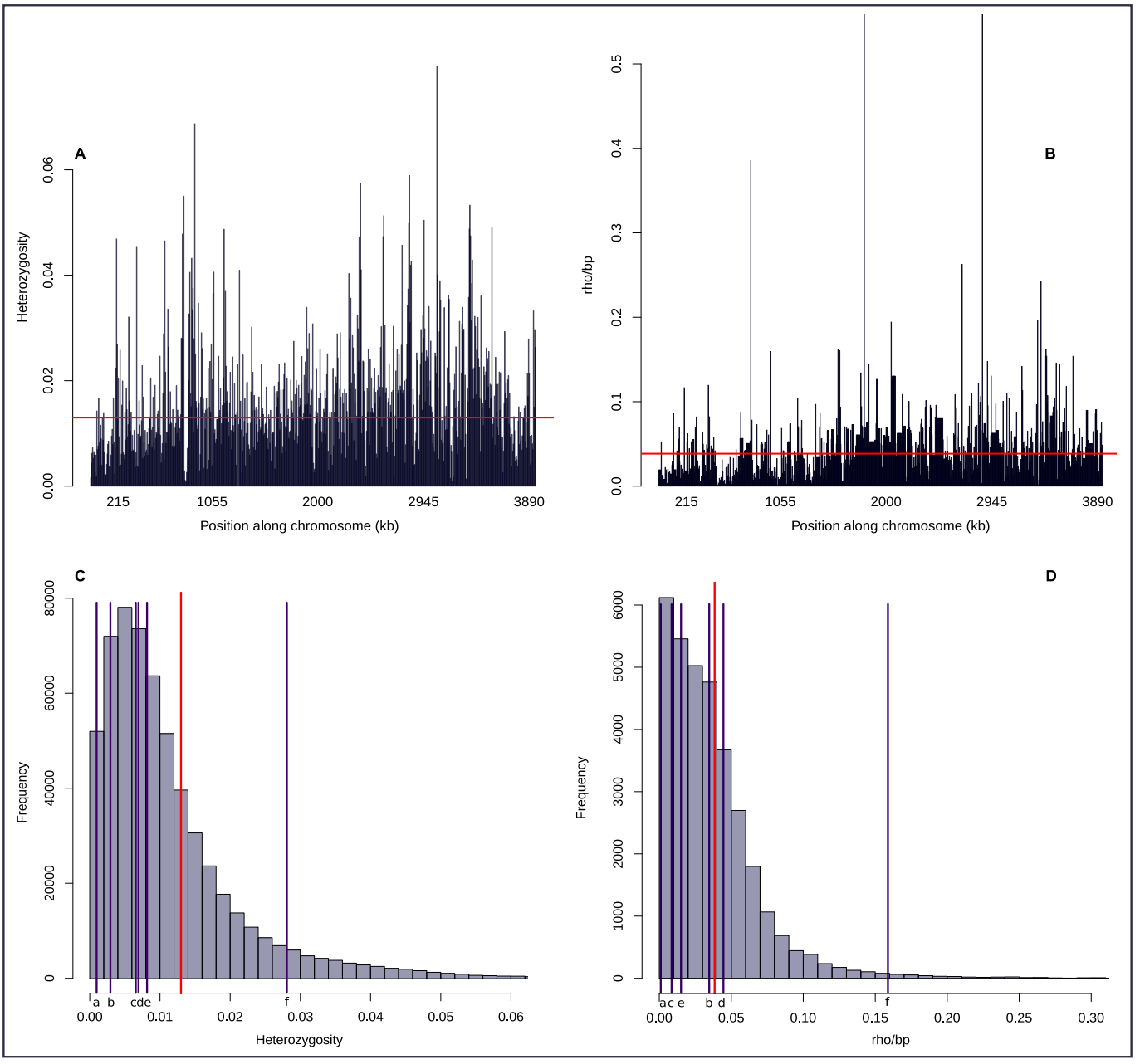
A
Heterozygosity
0.00
0.02
0.04
0.06
215
1055
2000
2945
3890
Position along chromosome (kb)
B
rho/bp
0.0
0.1
0.2
0.3
0.4
0.5
215
1055
2000
2945
3890
Position along chromosome (kb)
C
Frequency
0
20000
40000
60000
80000
a
b
cde
f
0.00
0.01
0.02
0.03
0.04
0.05
0.06
Heterozygosity
D
Frequency
0
1000
2000
3000
4000
5000
6000
a c e
b d
f
0.00
0.05
0.10
0.15
0.20
0.25
0.30
rho/bp

Figure S1: **Quantification of heterozygosity and estimation of ρ.**
Heterozygosity (A) and recombination (B) estimated along a representative contig (contig 110) and distribution of heterozygosity (C) and recombination rates (D) computed on 5000bp windows. Genome-wide average heterozygosity and recombination rate ρ are represented by a red bar. Other sexual species, taken from the literature, are depicted with a blue bar: a) *Homo sapiens* (*38*, *39*); b) *Gasterosteus aculeatus* (*40*); c) *Mus musculus* (*41*, *42*); d) *Drosophila melanogaster* (*20*); e) *Taenopygia guttata* (*43*); f) *Heliconius melpomene* (*44*, *45*).
The assembly comprises 218 contigs, a single representative is shown here. The rho and heterozygosity values for windows of 5000 base pairs for each of the 218 contigs are available in the zenodo archive: https://doi.org/10.5281/zenodo.8112093

Fig. S2

A

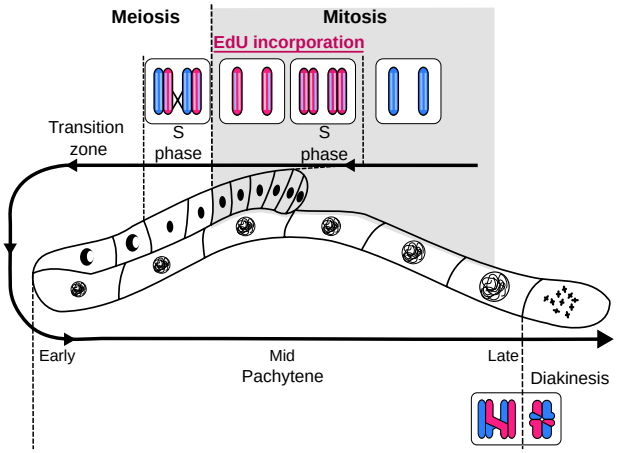

B

Mitosis					Meiosis		Occurency		Recombination is assessable?
	1st round		2nd round						
	S phase	Products	S phase	Products	S phase	Diakinesis	Theo.	Obs. (n)	
One mitotic division							1/2		Yes
	EdU incorporation						1/4		No
							1/4		No
							1/4	5	Yes
	EdU incorporation						1/4	1	No
							1/4	3	No
							1/8	12	Yes
							1/16	8*	No
							1/16		No

Figure S2: **Design and expectations for the Edu experiment**.
A) Design of EdU pulse-chase method. EdU is pink and DNA is blue. Sketch of *M. belari* gonad showing a pair of homologous chromosomes at each stage of oogenesis, with each chromatid and the two DNA strands per chromatids (Watson and Crick strands shown in light colors). Before EdU incorporation, each chromatid contains two unlabelled DNA strands (in light blue). Chromatids therefore appear blue. During the next S phase in the presence of EdU, the newly synthesized strains are pink. Hence, each chromatid appears pink. After chromatid segregation and a new S phase without EdU, one chromatid is entirely blue (because it has inherited the first unlabelled DNA strand and a new unlabelled DNA strand has been produced), whereas the other chromatid is pink (because although a new unlabelled DNA strand has been produced, it has inherited the labelled DNA strand from the previous cell cycle). The duration of the EdU exposure and progression through meiosis without EdU has been optimized to obtain such pattern. B) The analysis of chromosome colors at diakinesis strongly suggest that in fact, after the first S phase with EdU, the cells undergo two rounds of S phase in the absence of EdU.

Fig. S3

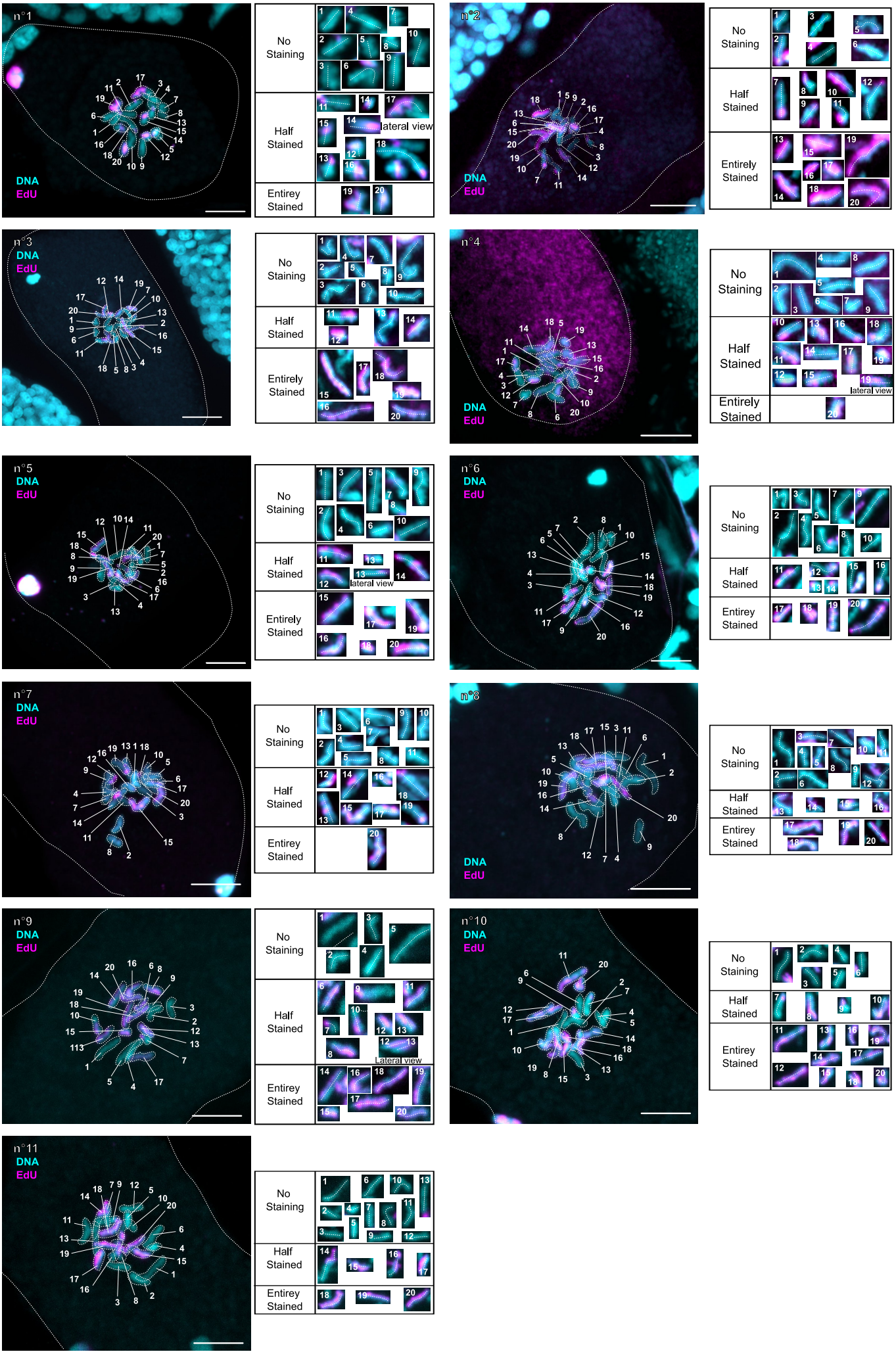
n°1
DNA
EdU
No Staining
Half Stained
lateral view
Entirey Stained
n°2
DNA
EdU
No Staining
Half Stained
Entirely Stained
n°3
DNA
EdU
No Staining
Half Stained
Entirely Stained
n°4
DNA
EdU
No Staining
Half Stained
lateral view
Entirely Stained
n°5
DNA
EdU
No Staining
Half Stained
lateral view
Entirey Stained
n°6
DNA
EdU
No Staining
Half Stained
Entirey Stained
n°7
DNA
EdU
No Staining
Half Stained
Entirey Stained
n°8
DNA
EdU
No Staining
Half Stained
Entirey Stained
n°9
DNA
EdU
No Staining
Half Stained
Lateral view
Entirey Stained
n°10
DNA
EdU
No Staining
Half Stained
Entirey Stained
n°11
DNA
EdU
No Staining
Half Stained
Entirey Stained

Figure S3: **Evidence of Directed Chromatid Assortment**.
11 images of fixed embryos at one-cell stage. EdU is in pink and DNA is in blue. The count of bicolored chromosomes is summarized in Figure 3. The dotted line shows the chromosome longest axis. Scale bar is 5 μm. Some chromosomes are shown twice, on the transverse and lateral view to better show the chromatid axis. The polar body (with labelled EdU chromatids, as expected) is visible in embryos #1 and #5. The sperm DNA (unlabeled) is visible in embryos # 3, #6 and #7.

Strain	Country	Location	Heterozygosity
JU2856	France	Angles-sur-l'Anglin. Indre	0.01381808
JU2859	United Kingdom	Cambridge	0.01531046
JU2817	France	Orsay	0.00735625
JU3129	United Kingdom	Coventry	0.01419700
JU3151	France	Saint-Aigny. Indre	0.01280673
JU3152	France	Saint-Aigny. Indre	0.01240229
JU3157	Germany	Heidelberg	0.01400762
JU3158	Germany	Heidelberg	0.01366134
JU3159	Germany	Postdam	0.01459582
JU3388	Ireland	Inis Mor. Aran Islands	0.01361719

Table S1: Measure of heterozygosity in 10 strains of *M. belari*

Supplementary Text

Population genomics and evolution of reproduction in *Mesorhabditis*

August 15, 2023

Contents

1 Population genetic structure under the *Mesorhabditis* life cycle

1.1 Model

1.1.1 General presentation and definition of parameters

The aim of the model is to predict population genomic patterns expected under the *Mesorhabditis* life cycle. We consider a single neutral locus with an infinite allele model (IAM) of mutation. We consider a subdivided population with K demes, each of size N. The total population is thus $N_T = KN$. The life cycle is as follows (Figure S4 redrawn from the main text). The generations are discrete and non-overlapping. Migration occurs before reproduction according to the island model at rate m. This simple population structure allows modelling the breeding structure of *Mesorhabditis* with high level of consanguineous mating: the lower the deme size and the migration rates, the higher the level of consanguineous mating.

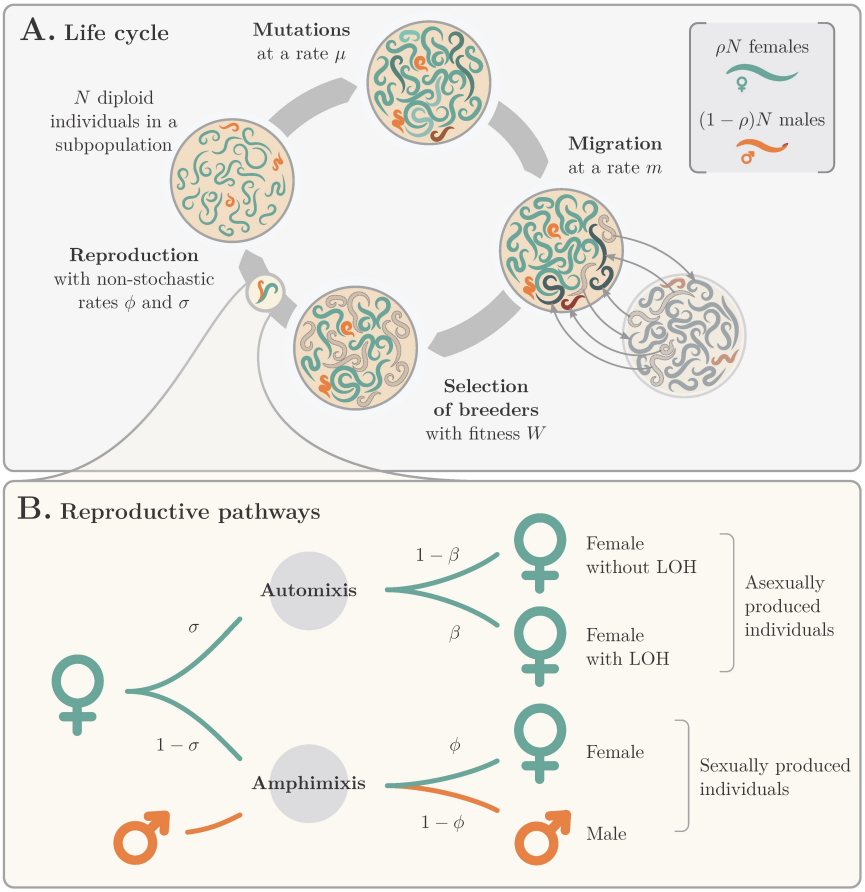

Figure S4: *Mesorhabditis* life cycle and parameters of the model.

Automictic reproduction that leads to gynogenetic females occurs in proportion σ and sexual reproduction $1-\sigma$. Under automixis, the rate of loss of heterozygosity (LOH) is β and depends on the underlying mechanism. With standard central fusion $\beta = 1/2$ after one crossover and random assortment of chromatids, and $\beta = 0$ if there is no recombination. In the proposed model of co-segregation of recombinant chromatids (CRC), $\beta = \frac{1}{2}(1-b)$, where b represents the segregation bias. If $b = 0$, there is no bias so that $\beta = 1/2$ as for recombinant chromatids under standard central fusion. If $b = 1$, the segregation is fully biased towards the co-segregation of the two recombinant chromatids. In this model, negative b values could also be considered, with $b = -1$ corresponding to complete LOH after one meiosis. However, we did not explore this possibility that is not relevant for the *Mesorhabditis* system. Under sexual reproduction, the proportion of females and males is ϕ and $1-\phi$, respectively. So far, no sexually-produced female has been observed (corresponding to ϕ=0). However, it is possible that they are produced at low rate in natural populations. If we set $\sigma = 1$ and $\beta = 0$, this is equivalent to a fully clonal model. If we set $\sigma = 0$ and $\phi = 1/2$, this is equivalent to a fully sexual model.

To obtain measures of genetic diversity and population structure (F-statistics) we derive recursions on a set of probabilities of identity by descent (IBD), Q_i, which leads to heterozygozity and F-statistics measure of the form [51]:

$$H_i = 1 - Q_i \tag{1}$$

and

$$F_{i,j} = \frac{Q_i - Q_j}{1 - Q_j} \tag{2}$$

To fully describe the model, we need to follow eight probabilities of IBD, noted Q_0^k when the two genes are sampled in the same individual, Q_1^k when they are sampled in two individuals of the same population, and Q_2^k, when they are sampled in two individuals from different populations. The superscript k stands for the sex of sampled individuals (see Figure S5).

From the parameters describing reproductive pathways (Figure S4) we obtain the proportion of males, sexual and gynogenetic females as:

$$\rho = (1-\sigma)(1-\phi) \tag{3a}$$

$$x_f = (1-\sigma)\phi \tag{3b}$$

$$x_g = \sigma \tag{3c}$$

from which we obtain the number of males and females in the populations and the proportions

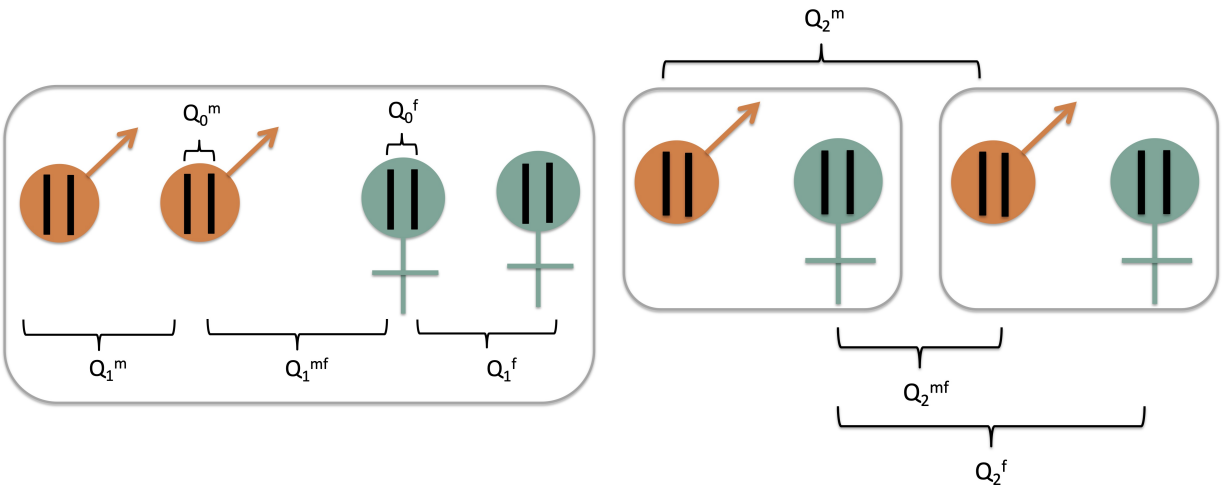

Figure S5: Definition of the eight probabilities of IBD. The grey boxes corresponds to demes.

of gynogenetic females among females

$$N_m = \rho N \tag{4a}$$
$$N_f = (1-\rho)N \tag{4b}$$
$$R_g = \frac{x_g}{x_g + x_f} \tag{4c}$$
$$\tag{4d}$$

We also need to introduce the following compound parameters:

$$\Upsilon = (1-u)^2 \tag{5a}$$
$$a = (1-m)^2 + \frac{m^2}{K-1} \tag{5b}$$
$$c = \frac{1-a}{K-1} \tag{5c}$$

Υ corresponds to the probability that the two sampled genes have not mutated in one generation, a, respectively b, corresponds to the probabilities that two individuals sampled in a same population, respectively in two different populations, were in the same population before migration.

1.1.2 Recursions

We now write the recursions of the $Q_i(t+1)$ as a function of the $Q_i(t)$. At equilibrium $Q_i(t+1) = Q_i(t)$ so we remove the time subscript and directly give the equations at

equilibrium:

$$Q_0^f = \Upsilon\big(R_g\big(\beta + (1-\beta)Q_0^f\big) + (1-R_g)Q_1^{mf}\big) \tag{6a}$$

$$Q_0^m = \Upsilon Q_1^{mf} \tag{6b}$$

$$\begin{aligned} Q_1^f = \Upsilon\Bigg(a\Bigg(&R_g^2\Bigg(\frac{1}{N_f}\big(\frac{1+Q_0^f}{2}\big) + \big(1-\frac{1}{N_f}\big)Q_1^f\Bigg) \\ &+ 2R_g(1-R_g)\Bigg(\frac{1}{2}\big(\frac{1}{N_f}\big(\frac{1+Q_0^f}{2}\big) + \big(1-\frac{1}{N_f}\big)Q_1^f\big) + \frac{Q_1^{mf}}{2}\Bigg) \\ &+ (1-R_g)^2\Bigg(\frac{1}{4}\big(\frac{1}{N_f}\big(\frac{1+Q_0^f}{2}\big) + \big(1-\frac{1}{N_f}\big)Q_1^f\big) + \frac{1}{4}\big(\frac{1}{N_m}\big(\frac{1+Q_0^m}{2}\big) + \big(1-\frac{1}{N_m}\big)Q_1^m\big) + \frac{1}{2}Q_1^{mf}\Bigg)\Bigg) \\ &+ \big(1-a\big)\Bigg(R_g^2Q_2^f + R_g(1-R_g)(Q_2^f + Q_2^{mf}) + (1-R_g)^2\big(\frac{Q_2^f}{4} + \frac{Q_2^m}{4} + \frac{Q_2^{mf}}{2}\big)\Bigg)\Bigg) \end{aligned} \tag{6c}$$

$$\begin{aligned} Q_1^m = \Upsilon\Bigg(a\Bigg(&\frac{1}{4}\big(\frac{1}{N_f}\big(\frac{1+Q_0^f}{2}\big) + \big(1-\frac{1}{N_f}\big)Q_1^f\big) + \frac{1}{4}\big(\frac{1}{N_m}\big(\frac{1+Q_0^m}{2}\big) + \big(1-\frac{1}{N_m}\big)Q_1^m\big) + \frac{1}{2}Q_1^{mf}\big)\Bigg) \\ &+ \big(1-a\big)\big(\frac{Q_2^f}{4} + \frac{Q_2^m}{4} + \frac{Q_2^{mf}}{2}\big)\Bigg) \end{aligned} \tag{6d}$$

$$\begin{aligned} Q_1^{mf} = \Upsilon\Bigg(a\Bigg(&R_g\Bigg(\frac{1}{2}\big(\frac{1}{N_f}\big(\frac{1+Q_0^f}{2}\big) + \big(1-\frac{1}{N_f}\big)Q_1^f\big) + \frac{Q_1^{mf}}{2}\Bigg) \\ &+ (1-R_g)\Bigg(\frac{1}{4}\big(\frac{1}{N_f}\big(\frac{1+Q_0^f}{2}\big) + \big(1-\frac{1}{N_f}\big)Q_1^f\big) + \frac{1}{4}\big(\frac{1}{N_m}\big(\frac{1+Q_0^m}{2}\big) + \big(1-\frac{1}{N_m}\big)Q_1^m\big) + \frac{Q_1^{mf}}{2}\Bigg)\Bigg) \\ &+ \big(1-a\big)\Bigg(R_g\big(\frac{Q_2^f}{2} + \frac{Q_2^{mf}}{2}\big) + (1-R_g)\big(\frac{Q_2^f}{4} + \frac{Q_2^m}{4} + \frac{Q_2^{mf}}{2}\big)\Bigg)\Bigg) \end{aligned} \tag{6e}$$

$$\begin{aligned} Q_2^f = \Upsilon\Bigg(c\Bigg(&R_g^2\Bigg(\frac{1}{N_f}\big(\frac{1+Q_0^f}{2}\big) + \big(1-\frac{1}{N_f}\big)Q_1^f\Bigg) \\ &+ 2R_g(1-R_g)\Bigg(\frac{1}{2}\big(\frac{1}{N_f}\big(\frac{1+Q_0^f}{2}\big) + \big(1-\frac{1}{N_f}\big)Q_1^f\big) + \frac{Q_1^{mf}}{2}\Bigg) \\ &+ (1-R_g)^2\Bigg(\frac{1}{4}\big(\frac{1}{N_f}\big(\frac{1+Q_0^f}{2}\big) + \big(1-\frac{1}{N_f}\big)Q_1^f\big) \\ &+ \frac{1}{4}\big(\frac{1}{N_m}\big(\frac{1+Q_0^m}{2}\big) + \big(1-\frac{1}{N_m}\big)Q_1^m\big) + \frac{Q_1^{mf}}{2}\big)\Bigg)\Bigg) \\ &+ \big(1-c\big)\Bigg(R_g^2Q_2^f + R_g(1-R_g)(Q_2^f + Q_2^{mf}) + (1-R_g)^2\big(\frac{Q_2^f}{4} + \frac{Q_2^m}{4} + \frac{Q_2^{mf}}{2}\big)\Bigg)\Bigg) \end{aligned} \tag{6f}$$

$$\begin{aligned} Q_2^m = \Upsilon\Bigg(c\Bigg(&\frac{1}{4}\big(\frac{1}{N_f}\big(\frac{1+Q_0^f}{2}\big) + \big(1-\frac{1}{N_f}\big)Q_1^f\big) \\ &+ \frac{1}{4}\big(\frac{1}{N_m}\big(\frac{1+Q_0^m}{2}\big) + \big(1-\frac{1}{N_m}\big)Q_1^m + \frac{Q_1^{mf}}{2}\Bigg) + \big(1-c\big)\big(\frac{Q_2^f}{4} + \frac{Q_2^m}{4} + \frac{Q_2^{mf}}{2}\big)\Bigg) \end{aligned} \tag{6g}$$

(continued on next page)

(continued from previous page)

$$Q_2^{mf} = \Upsilon\Bigg(c\Bigg(R_g\Bigg(\frac{1}{2}\Big(\frac{1}{N_f}\Big(\frac{1+Q_0^f}{2}\Big) + \Big(1-\frac{1}{N_f}\Big)Q_1^f\Big) + \frac{Q_1^{mf}}{2}\Bigg) + (1-R_g)\Bigg(\frac{1}{4}\Big(\frac{1}{N_f}\Big(\frac{1+Q_0^f}{2}\Big) + \Big(1-\frac{1}{N_f}\Big)Q_1^f\Big) + \frac{1}{4}\Big(\frac{1}{N_m}\Big(\frac{1+Q_0^m}{2}\Big) + \Big(1-\frac{1}{N_m}\Big)Q_1^m\Big) + \frac{Q_1^{mf}}{2}\Bigg)\Bigg) + \big(1-c\big)\Bigg(R_g\Big(\frac{Q_2^f}{2} + \frac{Q_2^{mf}}{2}\Big) + (1-R_g)\Big(\frac{Q_2^f}{4} + \frac{Q_2^m}{4} + \frac{Q_2^{mf}}{2}\Big)\Bigg)\Bigg) \tag{6d}$$

As an example, the rationale of the derivation is given for $Q_0^f(t+1)$. The two copies sampled in a female are IBD first if none has mutated (Υ). Then we must consider that this female is gynogenetic (R_g) or sexual ($1-R_g$). If it is gynogenetic, if heterozygozity has been lost (β) the two copies are IBD with probability one, otherwise ($1-\beta$) the probability of IBD is the same as for the mother, so $Q_0^f(t)$. If the female come from sexual reproduction, the two copies are IBD with the same probability as of a random male/female pair at the previous generation, Q_1^{mf}. The terms in $1/N_m$ and $1/N_f$ that appear in equations for the Q_1^k and Q_2^k correspond to the probability that two different individuals have the same father or mother, respectively.

This system of recursions can be written in the matrix form:

$$\vec{Q} = \Upsilon(\mathbf{G}\vec{Q} + \vec{C}) \tag{7}$$

where $\vec{Q}$ is the vector of probabilities of IBD,$\mathbf{G}$ is a matrix and $\vec{C}$ a vector, both depending of the parameters of the model. The solution can be written on the form:

$$\vec{Q} = (\mathbf{I} - \Upsilon\mathbf{G})^{-1}\Upsilon\vec{C} \tag{8}$$

where $\mathbf{I}$ is the identity matrix.

The F_{IS} statistics measured on genomic data corresponds to $F_{0,2}$ in our model as we compare the IBD of two gene copies sampled either within an individual or at random over the whole population. It can be defined either for males, females, or for the whole population

by weighting as a function of the sex-ratio:

$$F_{IS}^{m} = \frac{Q_0^m - Q_2^m}{1 - Q_2^m} \tag{9a}$$

$$F_{IS}^{f} = \frac{Q_0^f - Q_2^f}{1 - Q_2^f} \tag{9b}$$

$$F_{IS} = x_m \frac{Q_0^m - x_m Q_2^m - (1-x_m)Q_2^f}{1 - x_m Q_2^m - (1-x_m)Q_2^f} + (1-x_m)\frac{Q_0^f - x_m Q_2^m - (1-x_m)Q_2^f}{1 - x_m Q_2^m - (1-x_m)Q_2^f} \tag{9c}$$

1.1.3 Simulations

In addition to analytical derivations, an individual-based, multi-locus model was implemented using the SLiM software [50], where each individual's genome is explicitly defined. It allowed to simulate genomic patterns along a chromosome and to introduce deleterious mutations in the model. Each individual is represented by a unique pair of autosome. This chromosome consist of $L = 10^5$ loci, with a rate of recombination per locus r equal to $1/L = 10^{-5}$, so that on average one recombination event is observed per gametogenesis. Since *M. belari* has holocentric chromosomes (there is no specific centromere), the location of the chiasma is randomly drawn according to a uniform distribution along the chromosome. Two types of mutations are introduced, either neutral (no effect on fitness) or deleterious ones, with selection coefficient s, set to 0.01, and dominance coefficient h, set to 0.25, and acting multiplicatively across the genome. The life cycle was the same as described above. Various population sizes and migration rates were explored to modulate the level of inbreeding and we specifically studied the effect of the rate of production of sexual females, ϕ and the rate of LOH, β.

By adjusting the parameters of the model, we also compared the *M. belari* life cycle with more standard reproductive modes: full sexuality ($\sigma = 0$ and $\phi = 1/2$), full clonality ($\sigma = 1$ and $r = 0$), and central fusion automixis ($\sigma = 1$, and $\beta = 1/2$).

From the simulations we computed F_{IS} and the linkage-disequilibrium measure r^2 on neutral mutations at the scale of the whole population:

$$\mathrm{F_{IS}} = 1 - \frac{H_o}{H_e} \tag{10}$$

with H_o the observed heterozygosity (percentage of heterozygous sites) and H_e the expected heterozygosity :

$$H_e = \frac{2}{L}\sum_{i=1}^{n} f_i(1 - f_i) \tag{11}$$

a sum over all the n mutations present in the population with f_i their respective frequencies.

$$r^2 = \frac{D^2}{\pi_A \pi_a \pi_B \pi_b} \tag{12}$$

where $D = \pi_{AB} - \pi_A \pi_B$ with π_A and π_a the allelic frequency at a first locus A and π_B and π_b at a second locus B. Only mutations in frequency higher than 5% in the population were used. r^2 was calculated for pairs of loci as the function of their distance on the simulated chromosome.

1.2 Results

1.2.1 F_{IS}

The general solution of equation (8) can be obtained with the help of *Mathematica* [52] but it is formidable, so useless for direct biological interpretation. We thus performed numerical explorations in the general case. We also obtained approximations under two limit conditions: $\phi = 0$ (no sexually-produced females) and $\beta = 0$ (no LOH). Under these two conditions we also used the standard diffusion limit. First we used the following scaling parameters: $\theta = 4N_T u$, $\Phi = 2N_T \phi$, $B = 2N_T \beta$. Then, we assumed an infinite number of local populations so $K, N_T \to \infty$ but that the scaled parameters terms tends towards constant: $\theta, \Phi, B \to cte$. We also noted $M = 4Nm$, where migration is scaled with the local, N, which can be small.

Assuming no sexually-produced females we obtained:

$$F_{IS}^m \approx \frac{2B + \theta}{2(B + \theta) + M(\sigma B + \theta\sigma + 1)} \tag{13a}$$

$$F_{IS}^f \approx \frac{2B + M(\sigma B - 1)}{2(B + \theta) + M(\sigma B + \theta\sigma + 1)} \tag{13b}$$

$$F_{IS} \approx \frac{2B + \theta(1 - \sigma) + \sigma M(\sigma B - 1)}{2(B + \theta) + M(\sigma B + \theta\sigma + 1)} \tag{13c}$$

Assuming no LOH we obtained:

$$F_{IS}^m \approx \frac{(1 - \sigma)\Phi + \sigma\theta}{(1 - \sigma)\Phi(1 + M\sigma) + \sigma(2\theta + M(1 + \sigma\theta))} \tag{14a}$$

$$F_{IS}^f \approx \frac{(1 - \sigma)\Phi - \sigma M}{(1 - \sigma)\Phi(1 + M\sigma) + \sigma(2\theta + M(1 + \sigma\theta))} \tag{14b}$$

$$F_{IS} \approx \frac{(1 - \sigma)(\sigma\theta + \Phi) - M\sigma^2}{(1 - \sigma)\Phi(1 + M\sigma) + \sigma(2\theta + M(1 + \sigma\theta))} \tag{14c}$$

We give the three expressions for completeness but we can concentrate on the expression for the average F_{IS} In natural populations, there is a strong family structure with most

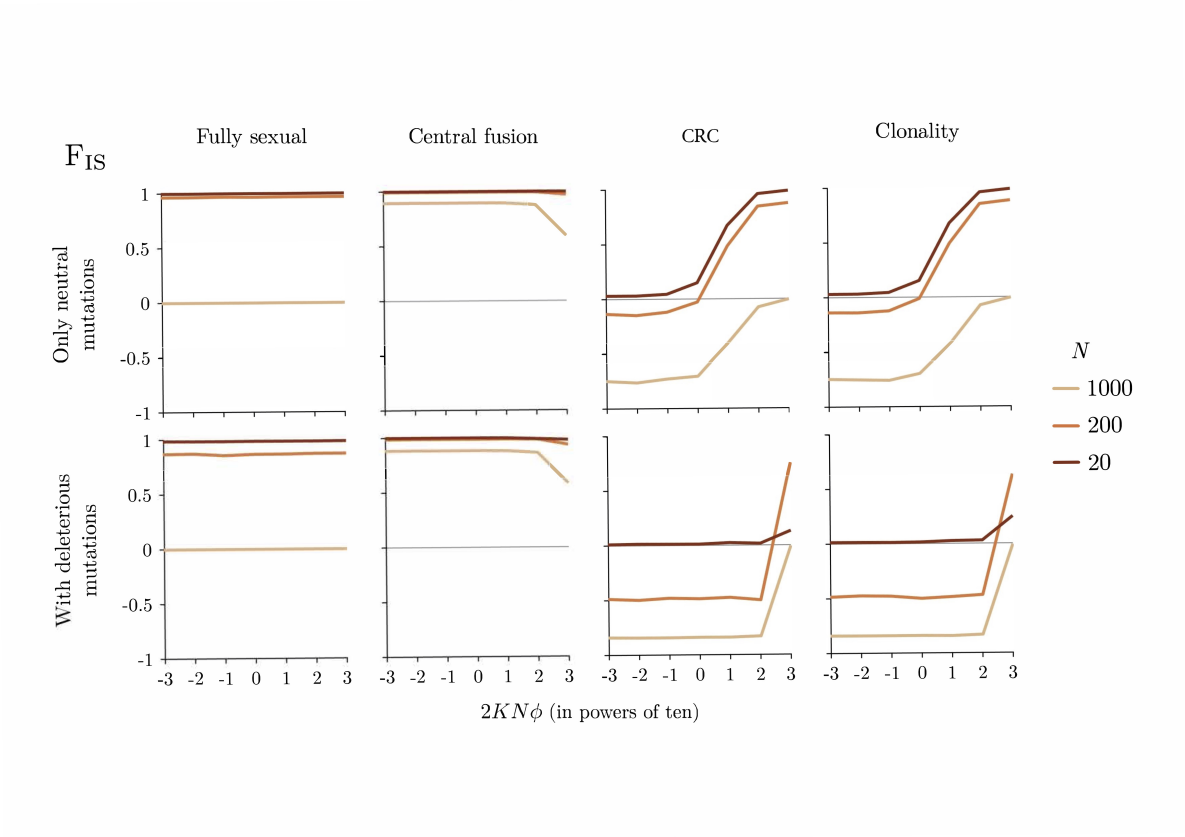

Figure S6: F_{IS} for the different reproductive modes as a function of the rate of sexually produced females ($2KN\phi$) for different levels of population structure ($KN = 1000$, so $N = 1000$ corresponds to a single populations and $N = 20$ to a highly structured one).

matings occurring between kins. In our model, it corresponds to low migration between demes, so M close to 0. Then, equations (13c) and (14c) become:

$$F_{IS} \approx \frac{2B + \theta(1-\sigma)}{2(B+\theta)} \tag{15}$$

$$F_{IS} \approx \frac{(1-\sigma)(\sigma\theta + \Phi)}{(1-\sigma)\Phi + 2\sigma\theta} \tag{16}$$

which both reduce to $F_{IS} = (1-\sigma)/2$ when $B = 0$ or $\Phi = 0$. As $\sigma \approx 0.9$ in natural populations it corresponds to $F_{IS} \approx 0.05$, so close to the observed value ($F_{IS} \approx 0.19$, see main text). In an unstructured population ($M \to \infty$, and see $N = 1000$ on Figure S6), F_{IS} tends to -1 with no LOH ($B = 0$) (see also [48]). Here, this is compensated by the strong family structure leading to F^f_{IS} close to 0 as illustrated on Figure S6 (see also [**?**]). It is worth noting that just a little bit of sex or LOH (higher than the mutation rate: $\phi, B > \theta$) rapidly leads to F^f_{IS} close to 1. This is confirmed by simulations as presented (Figure S6 and Figure

4 in the main text). This result is thus very sensitive to the occurrence of sexually produced females and to low level of LOH. For comparison, we also present the case of standard central fusion, clonality and fully sexual reproduction.

However, simulations showed that because of deleterious mutations, the range of parameters leading to F_{IS}^{f} close to 0 can be much wider, even when some females are sexually produced and when the CRC is not complete (Figure S7). This is explained by the selection against highly homozygous individuals. This is an important result as a non-zero proportion of sexually produced females is required to explain the low level of linkage disequilibrium observed genome wide as presented below.

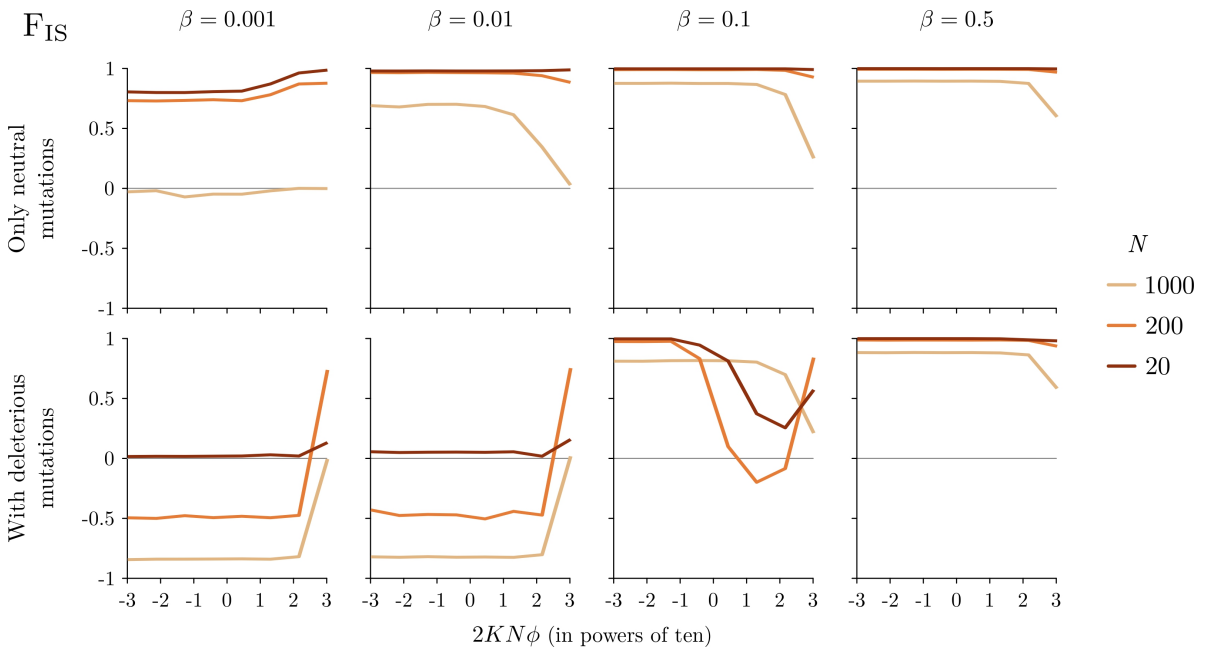

Figure S7: F_{IS} for automixis with different level of CRC ($\beta = 0$ corresponds to full co-segregation and $\beta = 1/2$ to random pairing).

For comparison, Figures S6 and S7 also shows the results for full sexuality, full clonality and standard central fusion automixis (without CRC).

1.2.2 Linkage disequilibrium

Analytical derivations for linkage disequilibrium would require recursion equations for 40 IBD probabilities. We thus only relied on simulations.

To understand the specific effect of the CRC we first considered a single unstructured population. As expected, LD is low and rapidly decreases with physical distance under sexual reproduction (Figure S8). In contrast, LD is high and independent of physical distance along chromosome under both full clonality because recombination does not occur, and

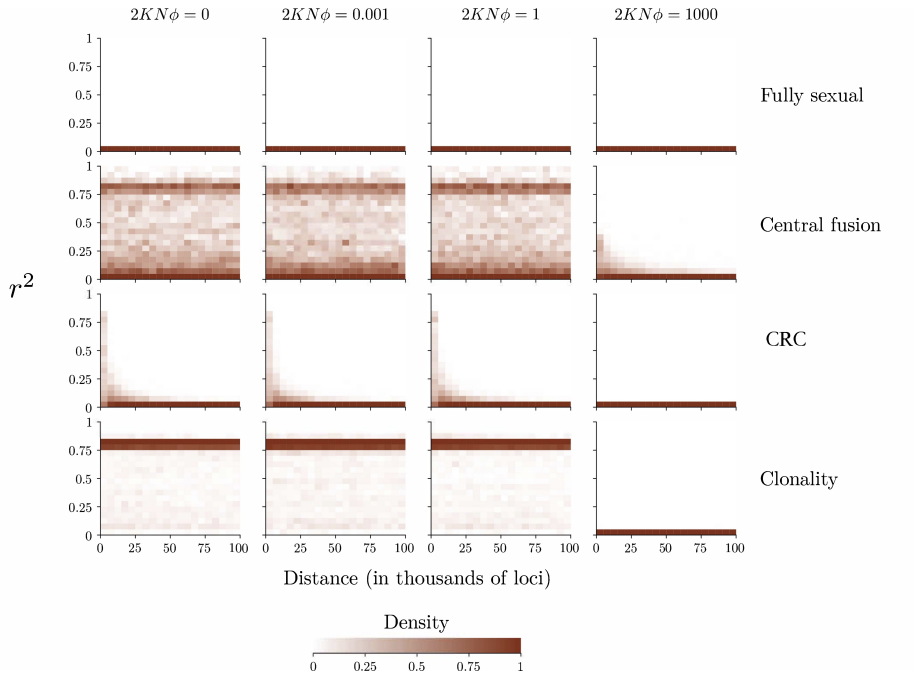

Figure S8: Pattern of linkage disequilibrium as a function of physical distance (in number of loci) for different rates of sexually produced females ($2NK\phi = 0.001, 1, 100$) and for different reproductive modes.

under standard central fusion because recombination is not efficient as individuals are mostly homozygotes. Under complete CRC and without sexually produced females, LD pattern is intermediate: much lower than under clonality or standard central fusion but higher than under full sexuality, and decreasing with physical distance (Figure S8). The reason is that, although new haplotypes are generated by recombination within individuals, they are never associated together through mating, so recombination is not as efficient as under full sexuality.

When we also consider the effect of population structure, LD is globally higher and the difference among reproductive modes are less clear under pure neutrality. However, when deleterious mutations are added the differences become stronger. In particular a very low rate of sexually produced females is sufficient to make CRC similar to full sexuality whereas much higher rates are necessary to erase the signature of clonality or standard central fusion (Figure S9).

1.2.3 Conclusion

Overall, the observed genomic pattern is well predicted by the strong family structure of *M. belari* populations directed chromatif assortment, sexually produced females at low rate (which can be unobserved in natural conditions), and the occurrence of deleterious mutations

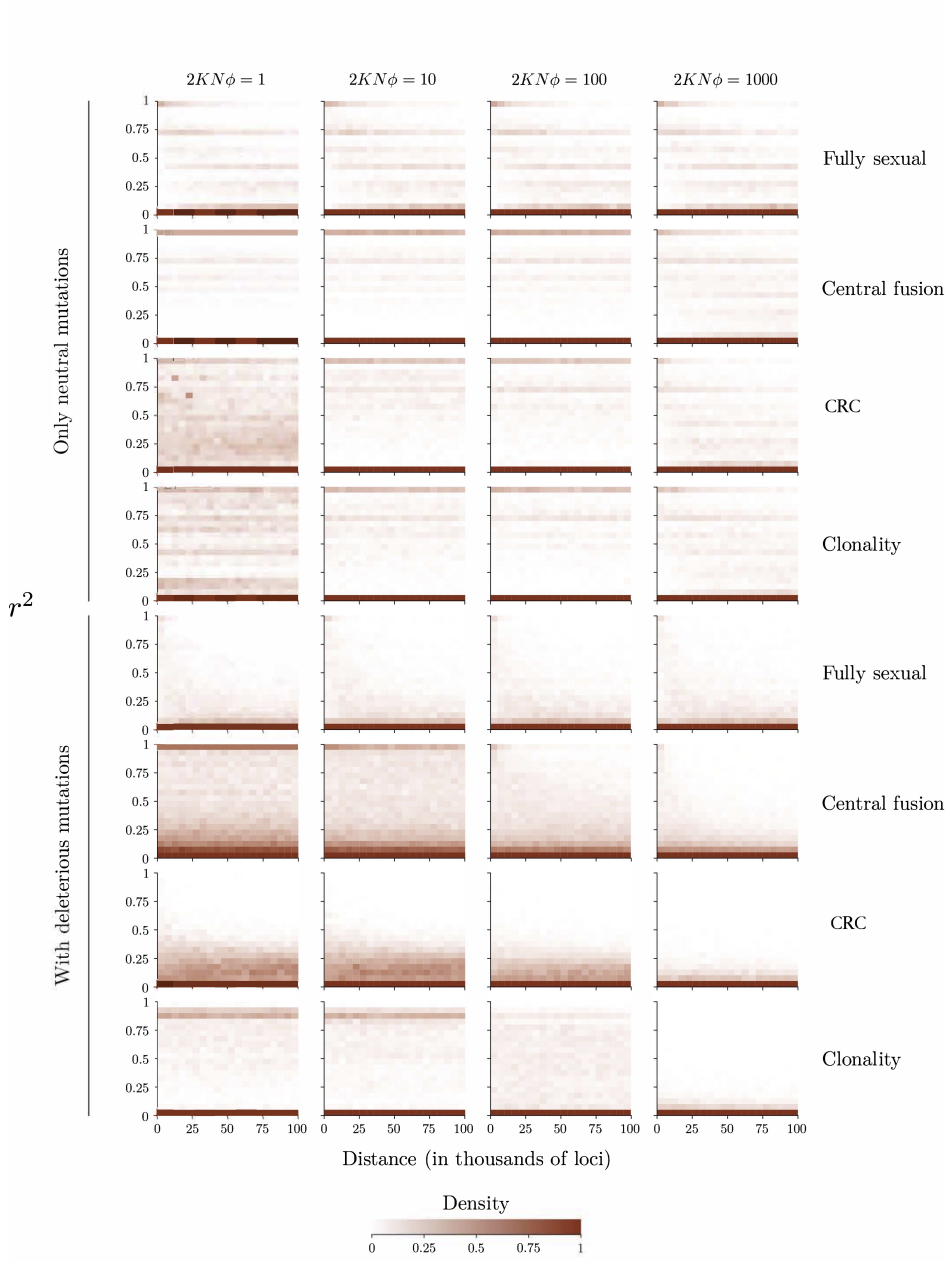

Figure S9: Pattern of linkage disequilibrium as a function of physical distance (in number of loci) for different rates of sexually produced females ($2NK\phi = 0.001, 1, 100$) and for different reproductive modes.

genome wide.

2 Evolution of the reproductive system

In the second model, we study the evolution of the atypical reproductive system of *M. belari* from a standard sexual population. Compared to the previous model, the parameters σ (proportion of asexually produced offspring) and β (rate of LOH during automixis) are no longer fixed but under the control of two independent evolving loci. Among sexually produced individuals the proportion of females is set to $\phi = 1/2$. Additional simulations where the sex-ratio can also evolve do not change the results and a sex ratio biased towards males evolved in a second step (not shown).

We started with a burn-in period where the population evolved under sexual reproduction. Then mutations are introduced at one or at the two loci controlling the reproductive mode. Each evolving locus is unlinked with any other locus. Transmission from parents to children of an evolving locus follows the same rules as transmission of loci on the focal chromosome, taking into account the potential LOH through chromosome segregation during automixis. It can take two different values, a resident value, g_r, or a mutant value, $g_m = g_r \pm \delta$. We used $\delta = 0.1$ to avoid too long simulations. We assumed additivity between the two alleles so the genotypic value is the sum of the two alleles. At the beginning of simulations, all individuals are homozygous for the resident allele and a mutant allele is randomly introduced in one individual of the population. If this mutant becomes fixed in the population, this mutant allele becomes the resident allele. If the mutant disappears, another mutant is directly reintroduced into the population at random.

2.1 Genotype to phenotype map

The value of σ and β are constrained between 0 and 1. The simulations start with a sexual population, with a rate of pseudogamy set to 0 and that can theoretically go up to 1. The rate of LOH β starts at 1/2 and can reach 0 (no LOH, complete cosegregation of recombinant chromatids) or 1 (full LOH, complete segregation of one recombinant and one non-recombinant chromatids). To map allelic values from $]-\infty, +\infty[$ to $[0, 1]$ we used the following functions:

$$P_\sigma = f(G_\sigma) \quad ; \quad P_\beta = \frac{1}{2}\left(1 - f(G_\beta)\right) \tag{17}$$

with

$$f(x) = \begin{cases} 1 - \left(1 - \frac{2}{\pi}\tan^{-1}(ax)\right)^b, & \text{if } g > 0 \\ \left(1 - \frac{2}{\pi}\tan^{-1}(-ax)\right)^b - 1, & \text{otherwise} \end{cases} \tag{18}$$

The parameters a and b define whether the function tends more or less quickly to 1 as x increases. We used $a = 0.1$ and $b = 15$ but equilibrium results are not sensitive to chosen

values. The rate of pseudogamy and the rate of LOH are controlled by the maternal genotype.

2.2 Inbreeding depression

The supposedly strong barrier to the evolution of asexuality (assuming that automixis mechanisms can emerge) is inbreeding depression (ID) due to LOH that leads to the exposure of recessive deleterious alleles. ID is calculated as $1 - w_1/w_0$ with w_0 being the fitness of sexually produced individuals and w_1 the fitness of asexually produced individuals.

A strong ID should hold back the evolution of automixis if the chromosome segregation bias is not strong, preventing LOH. Since we only modelled a single chromosome and central fusion leads to a LOH in only half of offsrpings, the maximum ID is 50%, which is the minimum value preventing the evolution of asexuality. Asexuality should always evolved under such a conditions. To allow a broader range of ID values we assumed an additional cost of LOH and corrected w_1 to $w_1^{corr} = (1-c)^{\beta(n-1)} w_1$, where n is the number of chromosomes (fixed to 10) and c is the mean fitness decline caused by LOH per chromosome.

2.3 Extinction-recolonisation cycle of subpopulations

In this model, a higher migration rate is set, allowing the evolving loci to be transmitted not too slowly from one population to another. It should also be noted that here the parameters controlling reproduction are no longer fixed rates. It is thus possible that populations may stochastically run out of males, especially if pseudogamy evolves and the percentage of males decreases. If a population has no more males, it becomes extinct. An extinct population is recolonised in the generation following its extinction by a male and at least one female randomly selected from the other population. This pair reproduces and together they form the next generation of the subpopulation.

REFERENCES AND NOTES

1. E. Suomalainen, A. Saura, J. Lokki, *Cytology and Evolution in Parthenogenesis* (CRC Press, 1987).

2. M. Neiman, T. F. Sharbel, T. Schwander, Genetic causes of transitions from sexual reproduction to asexuality in plants and animals. *J. Evol. Biol.* **27**, 1346–1359 (2014).

3. T. Lenormand, J. Engelstädter, S. E. Johnston, E. Wijnker, C. R. Haag, Evolutionary mysteries in meiosis. *Philos. Trans. R. Soc. Lond. B Biol. Sci.* **371**, 20160001 (2016).

4. M. Archetti, Complementation, genetic conflict, and the evolution of sex and recombination. *J. Hered.* **101**, S21–S33 (2010).

5. J. Engelstädter, Constraints on the evolution of asexual reproduction. *Bioessays* **30**, 1138–1150 (2008).

6. C. R. Haag, L. Theodosiou, R. Zahab, T. Lenormand, Low recombination rates in sexual species and sex-asex transitions. *Philos. Trans. R. Soc. Lond. B Biol. Sci.* **372**, 20160461 (2017).

7. K. S. Jaron, J. Bast, R. W. Nowell, T. R. Ranallo-Benavidez, M. Robinson-Rechavi, T. Schwander, Genomic features of parthenogenetic animals. *J. Hered.* **112**, 19–33 (2021).

8. A. Brandt, P. Tran Van, C. Bluhm, Y. Anselmetti, Z. Dumas, E. Figuet, C. M. François, N. Galtier, B. Heimburger, K. S. Jaron, M. Labédan, M. Maraun, D. J. Parker, M. Robinson-Rechavi, I. Schaefer, P. Simion, S. Scheu, T. Schwander, J. Bast, Haplotype divergence supports long-term asexuality in the oribatid mite *Oppiella nova*. *Proc. Natl. Acad. Sci. U.S.A.* **118**, e2101485118 (2021).

9. P. Simion, J. Narayan, A. Houtain, A. Derzelle, L. Baudry, E. Nicolas, R. Arora, M. Cariou, C. Cruaud, F. R. Gaudray, C. Gilbert, N. Guiglielmoni, B. Hespeels, D. K. L. Kozlowski, K. Labadie, A. Limasset, M. Llirós, M. Marbouty, M. Terwagne, J. Virgo, R. Cordaux, E. G. J. Danchin, B. Hallet, R. Koszul, T. Lenormand, J.-F. Flot, K. Van Doninck, Chromosome-level genome assembly reveals homologous chromosomes and recombination in asexual rotifer *Adineta vaga*. *Sci. Adv.* **7**, eabg4216 (2021).

10. P. Tran Van, Y. Anselmetti, J. Bast, Z. Dumas, N. Galtier, K. S. Jaron, K. Martens, D. J. Parker, M. Robinson-Rechavi, T. Schwander, P. Simion, I. Schön, First annotated draft genomes of nonmarine ostracods (Ostracoda, Crustacea) with different reproductive modes. *G3 (Bethesda)* **11**, jkab043 (2021).

11. H. Fradin, K. Kiontke, C. Zegar, M. Gutwein, J. Lucas, M. Kovtun, D. L. Corcoran, L. R. Baugh, D. H. A. Fitch, F. Piano, K. C. Gunsalus, Genome architecture and evolution of a unichromosomal asexual nematode. *Curr. Biol.* **27**, 2928–2939.e6 (2017).

12. R. Guidetti, M. Cesari, R. Bertolani, T. Altiero, L. Rebecchi, High diversity in species, reproductive modes and distribution within the *Paramacrobiotus richtersi* complex (Eutardigrada, Macrobiotidae). *Zool. Lett.* **5**, 1 (2019).

13. M. Grosmaire, C. Launay, M. Siegwald, T. Brugière, L. Estrada-Virrueta, D. Berger, C. Burny, L. Modolo, M. Blaxter, P. Meister, M.-A. Félix, P.-H. Gouyon, M. Delattre, Males as somatic investment in a parthenogenetic nematode. *Science* **363**, 1210–1213 (2019).

14. D. G. Albertson, J. N. Thomson, Segregation of holocentric chromosomes at meiosis in the nematode, *Caenorhabditis elegans*. *Chromosome Res.* **1**, 15–26 (1993).

15. D. E. Almanzar, S. G. Gordon, O. Rog, Meiotic sister chromatid exchanges are rare in *C. elegans*. *Curr. Biol.* **31**, 1499–1507.e3 (2021).

16. A.-C. Valfort, C. Launay, M. Sémon, M. Delattre, Evolution of mitotic spindle behavior during the first asymmetric embryonic division of nematodes. *PLOS Biol.* **16**, e2005099 (2018).

17. C. Launay, M.-A. Félix, J. Dieng, M. Delattre, Diversification and hybrid incompatibility in auto-pseudogamous species of *Mesorhabditis* nematodes. *BMC Evol. Biol.* **20**, 105 (2020).

18. T. S. Korneliussen, A. Albrechtsen, R. Nielsen, ANGSD: Analysis of next generation sequencing data. *BMC Bioinformatics* **15**, 356 (2014).

19. E. C. Andersen, J. P. Gerke, J. A. Shapiro, J. R. Crissman, R. Ghosh, J. S. Bloom, M.-A. Félix, L. Kruglyak, Chromosome-scale selective sweeps shape *Caenorhabditis elegans* genomic diversity. *Nat. Genet.* **44**, 285–290 (2012).

20. A. H. Chan, P. A. Jenkins, Y. S. Song, Genome-wide fine-scale recombination rate variation in *Drosophila melanogaster*. *PLOS Genet.* **8**, e1003090 (2012).

21. F. Balloux, L. Lehmann, T. de Meeûs, The population genetics of clonal and partially clonal diploids. *Genetics* **164**, 1635–1644 (2003).

22. S. L. Ament-Velásquez, E. Figuet, M. Ballenghien, E. E. Zattara, J. L. Norenburg, F. A. Fernández-Álvarez, J. Bierne, N. Bierne, N. Galtier, Population genomics of sexual and asexual lineages in fissiparous ribbon worms (Lineus, Nemertea): Hybridization, polyploidy and the Meselson effect. *Mol. Ecol.* **25**, 3356–3369 (2016).

23. S. Glémin, N. Galtier, Genome evolution in outcrossing versus selfing versus asexual species. *Methods Mol. Biol.* **855**, 311–335 (2012).

24. M. Mandrioli, G. C. Manicardi, Holocentric chromosomes. *PLOS Genet.* **16**, e1008918 (2020).

25. M. P. H. Stumpf, G. A. T. McVean, Estimating recombination rates from population-genetic data. *Nat. Rev. Genet.* **4**, 959–968 (2003).

26. A. Agostinho, B. Meier, R. Sonneville, M. Jagut, A. Woglar, J. Blow, V. Jantsch, A. Gartner, Combinatorial regulation of meiotic holliday junction resolution in *C. elegans* by HIM-6 (BLM) helicase, SLX-4, and the SLX-1, MUS-81 and XPF-1 nucleases. *PLOS Genet.* **9**, e1003591 (2013).

27. N. J. O'Neil, J. S. Martin, J. L. Youds, J. D. Ward, M. I. R. Petalcorin, A. M. Rose, S. J. Boulton, Joint molecule resolution requires the redundant activities of MUS-81 and XPF-1 during *Caenorhabditis elegans* meiosis. *PLOS Genet.* **9**, e1003582 (2013).

28. Y. Hong, M. Velkova, N. Silva, M. Jagut, V. Scheidt, K. Labib, V. Jantsch, A. Gartner, The conserved LEM-3/Ankle1 nuclease is involved in the combinatorial regulation of meiotic recombination repair and chromosome segregation in *Caenorhabditis elegans*. *PLOS Genet.* **14**, e1007453 (2018).

29. Y. Liu, C. F. Nielsen, Q. Yao, I. D. Hickson, The origins and processing of ultra fine anaphase DNA bridges. *Curr. Opin. Genet. Dev.* **26**, 1–5 (2014).

30. B. P. Oldroyd, B. Yagound, M. H. Allsopp, M. J. Holmes, G. Buchmann, A. Zayed, M. Beekman, Adaptive, caste-specific changes to recombination rates in a thelytokous honeybee population. *Proc. R. Soc. B Biol. Sci.* **288**, 20210729 (2021).

31. E. Altendorfer, L. I. Láscarez-Lagunas, S. Nadarajan, I. Mathieson, M. P. Colaiácovo, Crossover position drives chromosome remodeling for accurate meiotic chromosome segregation. *Curr. Biol.* **30**, 1329–1338.e7 (2020).

32. G. Taberly, [The cytology of parthenogenesis in *Platynothrus peltifer* (Koch) (Acarien, Oribate)]. *C. R. Hebd. Seances Acad. Sci.* **247**, 1655–1657 (1958).

33. M. Archetti, Evidence from automixis with inverted meiosis for the maintenance of sex by loss of complementation. *J. Evol. Biol.* **35**, 40–50 (2022).

34. M. Schvarzstein, S. M. Wignall, A. M. Villeneuve, Coordinating cohesion, co-orientation, and congression during meiosis: Lessons from holocentric chromosomes. *Genes Dev.* **24**, 219–228 (2010).

35. M. Sarens, G. P. Copenhaver, N. De Storme, The role of chromatid interference in determining meiotic crossover patterns. *Front. Plant Sci.* **12**, 656691 (2021).

36. K. J. Beumer, S. Pimpinelli, K. G. Golic, Induced chromosomal exchange directs the segregation of recombinant chromatids in mitosis of *Drosophila*. *Genetics* **150**, 173–188 (1998).

37. C. S. Ottolini, L. Newnham, A. Capalbo, S. A. Natesan, H. A. Joshi, D. Cimadomo, D. K. Griffin, K. Sage, M. C. Summers, A. R. Thornhill, E. Housworth, A. D. Herbert, L. Rienzi, F. M. Ubaldi, A. H. Handyside, E. R. Hoffmann, Genome-wide maps of recombination and chromosome segregation in human oocytes and embryos show selection for maternal recombination rates. *Nat. Genet.* **47**, 727–735 (2015).

38. P. R. Oxley, L. Ji, I. Fetter-Pruneda, S. K. McKenzie, C. Li, H. Hu, G. Zhang, D. J. C. Kronauer, The genome of the clonal raider ant *Cerapachys biroi*. *Curr. Biol.* **24**, 451–458 (2014).

39. M. Dukić, D. Berner, C. R. Haag, D. Ebert, How clonal are clones? A quest for loss of heterozygosity during asexual reproduction in *Daphnia magna*. *J. Evol. Biol.* **32**, 619–628 (2019).

40. L. Serra, D. Z. Chang, M. Macchietto, K. Williams, R. Murad, D. Lu, A. R. Dillman, A. Mortazavi, Adapting the Smart-seq2 protocol for robust single worm RNA-seq. *Bio. Protoc.* **8**, e2729 (2018).

41. H. Li, R. Durbin, Fast and accurate short read alignment with Burrows-Wheeler transform. *Bioinformatics* **25**, 1754–1760 (2009).

42. H. Li, B. Handsaker, A. Wysoker, T. Fennell, J. Ruan, N. Homer, G. Marth, G. Abecasis, R. Durbin; 1000 Genome Project Data Processing Subgroup, The sequence alignment/map format and SAMtools. *Bioinformatics* **25**, 2078–2079 (2009).

43. A. M. Bolger, M. Lohse, B. Usadel, Trimmomatic: A flexible trimmer for Illumina sequence data. *Bioinformatics* **30**, 2114–2120 (2014).

44. M. G. Grabherr, B. J. Haas, M. Yassour, J. Z. Levin, D. A. Thompson, I. Amit, X. Adiconis, L. Fan, R. Raychowdhury, Q. Zeng, Z. Chen, E. Mauceli, N. Hacohen, A. Gnirke, N. Rhind, F. di Palma, B. W. Birren, C. Nusbaum, K. Lindblad-Toh, N. Friedman, A. Regev, Full-length transcriptome assembly from RNA-Seq data without a reference genome. *Nat. Biotechnol.* **29**, 644–652 (2011).

45. P. Gayral, J. Melo-Ferreira, S. Glémin, N. Bierne, M. Carneiro, B. Nabholz, J. M. Lourenco, P. C. Alves, M. Ballenghien, N. Faivre, K. Belkhir, V. Cahais, E. Loire, A. Bernard, N. Galtier, Reference-free population genomics from next-generation transcriptome data and the vertebrate-invertebrate gap. *PLOS Genet.* **9**, e1003457 (2013).

46. M. Patterson, T. Marschall, N. Pisanti, L. van Iersel, L. Stougie, G. W. Klau, A. Schönhuth, WhatsHap: Weighted haplotype assembly for future-generation sequencing reads. *J. Comput. Biol.* **22**, 498–509 (2015).

47. B. L. Browning, X. Tian, Y. Zhou, S. R. Browning, Fast two-stage phasing of large-scale sequence data. *Am. J. Hum. Genet.* **108**, 1880–1890 (2021).

48. J. Engelstädter, Asexual but not clonal: Evolutionary processes in automictic populations. *Genetics* **206**, 993–1009 (2017).

49. F. Prugnolle, T. De Meeus, Apparent high recombination rates in clonal parasitic organisms due to inappropriate sampling design. *Heredity* **104**, 135–140 (2010).

50. B. C. Haller, P. W. Messer, SLiM 3: Forward genetic simulations beyond the wright-fisher model. *Mol. Biol. Evol.* **36**, 632–637 (2019).

51. F. Rousset, *Genetic Structure and Selection in Subdivided Populations* (Princeton Univ. Press, 2004), vol. 40.

52. Wolfram-Research Inc., *Mathematica Edition: Version 8.0* (Wolfram Research, 2010).